Journal of Materials Chemistry B

REVIEW

View Article Online
View Journal

Cite this: DOI: 10.1039/d6tb00661b

From materials to medicine: formulation-driven optimization and clinical prospects of NIR-II optical imaging agents

Junjie Zou,†[a] Lijuan Yang,†[a] Wenxiang Zhang,†[c] Gang Liu *[a] and Zhixiang Lu *[b]

Conventional optical imaging is constrained by photon absorption and multiple scattering in biological tissues. Extending excitation and emission into the second near-infrared window (NIR-II, 1000–1700 nm) markedly suppresses tissue autofluorescence and improves imaging fidelity. However, enhanced optical performance alone does not ensure clinical translatability. In this review, we distinguish the conceptual boundary between optical probes and translational optical agents, highlighting the critical role of formulation engineering in bridging material functionality with biomedical applicability. Representative NIR-II probe classes are summarized together with their intrinsic advantages and translational limitations. We further discuss key formulation strategies for optical agent construction, including targeting engineering, hydrophilicity regulation, size optimization, and carrier-assisted integration. Recent advances in cardiovascular, oncological, neurological, and multimodal imaging applications are also reviewed. Finally, remaining challenges related to biosafety, imaging hardware, and clinical standardization are discussed. By adopting a formulation-centered perspective, this review emphasizes the transition from signal-generating probes to clinically relevant optical agents and outlines future directions for accelerating the translation of NIR-II imaging toward precision diagnostics and image-guided medicine.

Received 24th March 2026,
Accepted 27th May 2026

DOI: 10.1039/d6tb00661b

rsc.li/materials-b

1. Introduction

Clinical imaging techniques are widely used for disease diagnosis and monitoring, surgical guidance, and evaluation of therapeutic efficacy and prognosis.[1] With the advancement of science and technology, various imaging modalities have been adopted in clinical practice, including computed tomography (CT), magnetic resonance imaging (MRI), positron emission tomography (PET), and single-photon emission computed tomography (SPECT). However, these tomographic techniques are limited by several inherent drawbacks: exposure to harmful ionizing radiation (in CT, PET, and SPECT), poor spatial resolution (in MRI and PET), low temporal resolution due to the reliance on image reconstruction (in CT, MRI, PET, and SPECT), and a lack of suitable exogenous or endogenous probes for molecular or functional imaging.[2]

Optical imaging, combined with specialized optical probes, offers high spatiotemporal resolution, deep tissue penetration, and real-time monitoring capabilities, making it highly promising for both basic biomedical research and clinical applications.[3] Among optical imaging modalities, near-infrared (NIR) fluorescence imaging has attracted significant attention due to its superior tissue penetration,[4] low autofluorescence background, and high spatial resolution.[5] Numerous studies have demonstrated its effectiveness in imaging the vascular system,[6,7] lymphatic system,[8] and tumors.[9] It is widely accepted in the scientific community that the spectral range from 1000 nm to 1700 nm defines the NIR-II window. Compared with the NIR-I window, NIR-II fluorescence imaging features lower tissue autofluorescence, deeper tissue penetration, and higher signal-to-noise ratio (SNR, a quantitative parameter describing the ratio between the desired signal and background noise, reflecting the clarity and reliability of an imaging or detection system).[10] In 2021, Qian *et al.*[11–13] conducted comprehensive simulations and *in vivo* imaging studies across the entire NIR spectrum, expanding the NIR-II window to 900–1880 nm (Fig. 1a). NIR-II imaging

[a] State Key Laboratory of Vaccines for Infectious Diseases, Xiang An Biomedicine Laboratory, Fujian Engineering Research Center of Molecular Theranostic Technology, Center for Molecular Imaging and Translational Medicine, School of Public Health, Xiamen University, Xiamen, Fujian, 361102, China. E-mail: gangliu.cmitm@xmu.edu.cn
[b] State Key Laboratory of Vaccines for Infectious Diseases & Fujian Provincial Key Laboratory of Innovative Drug Target Research, School of Pharmaceutical Sciences, Xiamen University, Xiamen 361102, China. E-mail: zhixiangl@xmu.edu.cn
[c] State Key Laboratory of Molecular Vaccinology and Molecular Diagnostics, State Key Laboratory of Vaccines for Infectious Diseases, Center for Molecular Imaging and Translational Medicine, Xiang An Biomedicine Laboratory, School of Life Sciences, Xiamen University, Xiamen, Fujian 361102, China
† Junjie Zou, Lijuan Yang and Wenxiang Zhang contributed equally to this work.

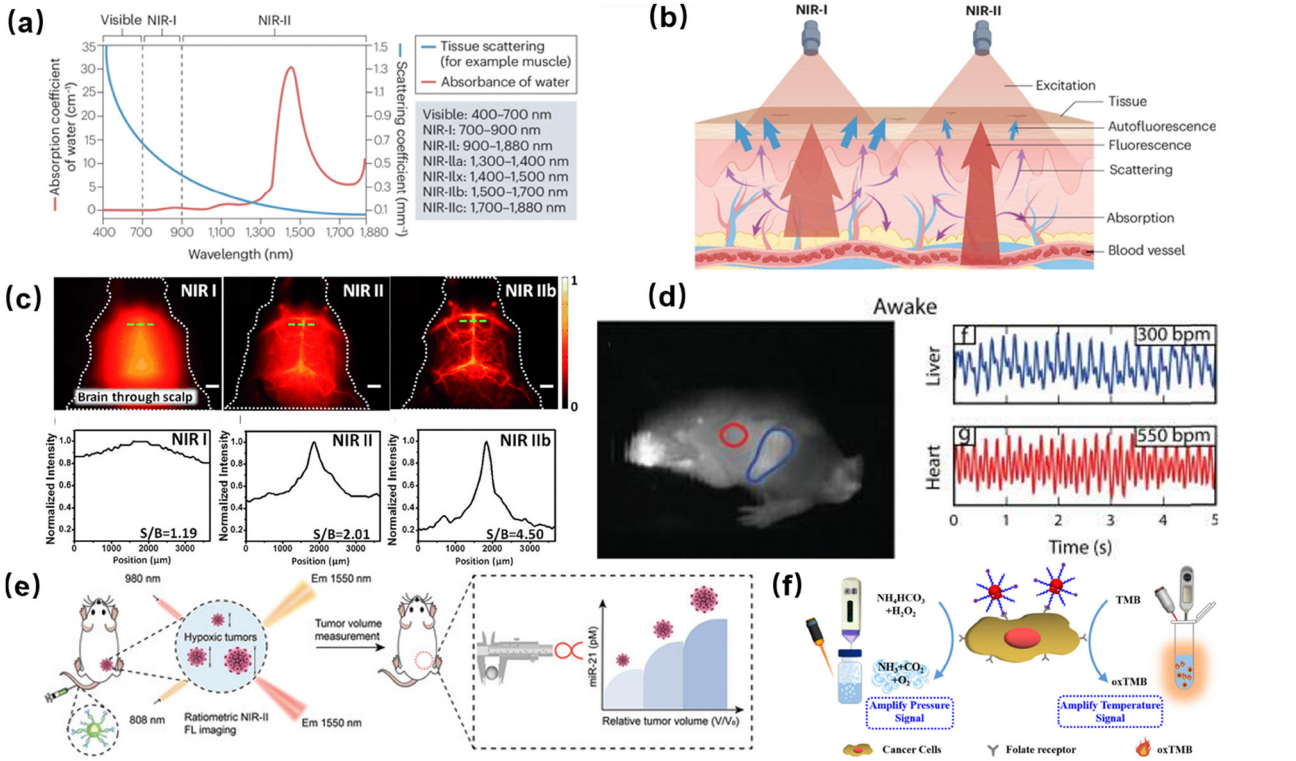

Fig. 1 (a) NIR-II enables clearer imaging with reduced scattering. Copyright 2024, Springer Nature.[18] (b) NIR-II imaging enhances visualization and surgical precision. Copyright 2024, Springer Nature.[18] (c) NIR-IIb yields superior cerebrovascular imaging clarity. Copyright 2015, John Wiley and Sons.[14] (d) SWIR imaging enables noninvasive vital monitoring. Copyright 2017, Springer Nature.[15] (e) Ratiometric NIR-II probe monitors miR-21 and cancer. Copyright 2024, John Wiley and Sons.[16] (f) Schematic of pressure and temperature sensing platforms. Copyright 2021, American Chemical Society.[17]

provides several unique advantages for clinical diagnostics, including high spatial resolution, non-invasiveness, real-time monitoring, portability, and operational simplicity (Fig. 1b). High Resolution: within the NIR-II spectral range, photon scattering in biological tissues is markedly attenuated, shifting light transport away from a fully diffusive regime toward quasi-linear propagation. Consequently, the image degradation caused by multiple light scattering is substantially reduced. Moreover, endogenous autofluorescence—which is prominent in NIR-I window—becomes negligible at longer NIR-II wavelengths. Together, these effects suppress background interference, leading to significantly improved SNR and enhanced spatial resolution during deep-tissue imaging (Fig. 1c).[14] It should be noted, however, that the extent of this improvement depends on tissue heterogeneity and instrumental sensitivity, factors that vary across experimental settings. Non-invasiveness: unlike many conventional diagnostic techniques that require surgical intervention or physical contact, optical imaging can be performed without incision or direct tissue interaction, thereby minimizing procedural risk and patient discomfort. Demonstrating this potential, Bawendi and colleagues developed short-wave infrared-emitting InAs quantum dots for non-contact, whole-body imaging in awake mice, while simultaneously monitoring resting physiological parameters (Fig. 1d).[15] Although such studies highlight the practical benefits of NIR-II imaging, questions regarding probe scalability and long-term biocompatibility remain to be addressed. Real-time monitoring: optical imaging further enables dynamic, real-time visualization of biomolecular processes in living systems. This temporal capability allows for early detection of pathological changes and supports molecular-level disease assessment. Nevertheless, real-time monitoring presents methodological challenges: signal instability, motion artifacts, and limited photostability of probes can complicate longitudinal measurements. Therefore, translating real-time optical data into quantitative diagnostic conclusions requires careful interpretation. For example, while NIR imaging has been used for early detection of skin and breast cancers—by visualizing vascular patterns and microcirculation—such applications must account for the technical constraints inherent to dynamic imaging. Yang *et al.*[16] developed a NIR-II ratiometric fluorescent nanoplatform (DCNP@DNA2@IR806) capable of real-time, quantitative visualization of miR-21 expression *in vivo* in tumor-bearing mice. Using this system, miR-21 abundance was shown to closely track tumor growth and neovascularization, highlighting its potential utility for early-stage cancer diagnosis and longitudinal assessment of tumor progression (Fig. 1e). Portability and simplicity: current cancer cell detection methods based on electrochemical, fluorescent, chemiluminescent, magnetic, Raman, mass spectrometry, microfluidic, and colorimetric

readouts often suffer from high cost, complexity, and dependence on large-scale instrumentation, limiting their applicability in point-of-care settings. Wang *et al.*[17] reported the fabrication of NIR-II-responsive gold nanoframes (Au NFs) through a combined photoreduction and template-etching strategy. When coupled with portable pressure and temperature sensing devices, these nanomaterials facilitated highly sensitive, dual-modal cancer cell detection, underscoring their potential for early oncological screening and real-time prognostic evaluation (Fig. 1f).

Optical diagnostic technologies are increasingly adopted in clinical practice, enhancing diagnostic accuracy while minimizing procedural invasiveness. This progress is fundamentally linked to the rational design of optical probes. When it comes to optical probes, it is important to distinguish between an optical ''probe'' and an optical ''agent'' of biomedical imaging. In general, a probe refers to a molecule, fluorophore, or nanomaterial possessing intrinsic optical responsiveness or signal-generation capability. Most studies on probes primarily focus on optical performance parameters such as absorption characteristics, emission wavelength, quantum yield, or photostability. However, favorable optical properties alone do not necessarily guarantee biomedical applicability or clinical translation.

In contrast, an optical agent represents a formulation-engineered system developed from optical probes with additional consideration of *in vivo* behavior and translational feasibility. Beyond signal generation, optical agents are typically designed to address physiological stability, aqueous dispersibility, biosafety, pharmacokinetics, targeting efficiency, immune compatibility, large-scale manufacturability, and long-term storage stability. Therefore, the transition from a probe to an agent is not merely a semantic difference, but reflects a critical evolution from material functionality toward clinically applicable biomedical systems.

In biomedical imaging, probes act as signal converters, transforming the recognition of specific biomarkers into detectable optical outputs. Many clinically established small-molecule fluorophores, such as the FDA-approved NIR-I dye indocyanine green (ICG), are characterized by well-defined chemical structures and predictable pharmacokinetics—properties that often weigh more heavily in regulatory approval than optical performance alone. Notably, ICG has garnered renewed interest due to its non-negligible emission extending into the NIR-II window. From a formulation perspective, optical agents refer to probes or materials engineered not only for optimal optical properties but also for biological compatibility. Advancing from a molecular probe to a formulated agent can address inherent limitations such as instability and undesirable biodistribution, thereby extending functional utility *in vivo*. Within the NIR-II domain, nanoprobes are often functionalized with targeting moieties—including antibodies, peptides, nucleic acids, or biomimetic membranes—to enable active targeting. This strategy enhances precise lesion localization and creates opportunities for earlier diagnosis and targeted therapy. Representative cases illustrate how deliberate formulation can directly expand clinical applicability. Zhu *et al.*[19] enhanced ICG by conjugating it with functionalized albumin. This formulation unexpectedly extended the effective imaging window to approximately 3 hours—a stark contrast to the rapid signal decay of free ICG ($\sim$2 minutes)—while enabling high-resolution visualization of microvasculature. In a distinct strategy focused on combination therapy, Zhang *et al.*[20] co-encapsulated cisplatin and ICG within gelatin-based nanocapsules. This design established an NIR-II fluorescence-guided platform for the precise chemoradiotherapy of treatment-resistant benign lesions. Similarly, Yang *et al.*[21] developed a biomimetic nanoplatform by coating a doxorubicin-loaded polymeric core, integrated with DSPE-PEG2000-modified ICG, with cancer cell membranes. The resulting construct demonstrated effective tumor-homing capability and high photothermal conversion efficiency, highlighting the functional benefits of membrane-mediated targeting for combined chemo-photothermal therapy. While these innovative formulations demonstrate significant functional advantages in preclinical models, their increased structural complexity raises important translational questions. Challenges related to scalable manufacturing, batch-to-batch reproducibility, and long-term biosafety continue to define the practical limits of NIR-II optical agent development.

Optical imaging technologies hold significant and growing clinical value in disease diagnosis, treatment guidance, and biomarker detection. These modalities provide high-resolution visualization, enabling more precise delineation of tumor boundaries and lesion extent. Such clarity directly informs critical clinical decisions, including surgical resection margins and radiotherapy planning. Against this backdrop, techniques offering enhanced resolution at the tissue level are of particular interest. One notable advancement is dynamic full-field optical coherence tomography (D-FFOCT), which has emerged as a high-resolution method capable of capturing subtle, functional contrasts within tissues. Wang *et al.*[22] were the first to apply D-FFOCT to image breast tissue and axillary lymph nodes, producing ''virtual histology'' images that closely resemble traditional pathological sections. Notably, clinicians demonstrated reliable interpretability of these label-free, non-sectioned images after only minimal training. This capability is largely attributed to the inherent metabolic and structural contrasts between malignant and normal tissues captured by the technique. However, whether such pattern recognition can be consistently generalized across diverse tumor types remains an open question for further validation.

Beyond morphological assessment, optical imaging allows direct visualization of vascular architecture and hemodynamic activity, facilitating the precise localization of thrombotic lesions. Illustrating this capability, Tang *et al.*[23] developed a high-efficiency NIR-II contrast agent named 4THTPB, which enabled high-fidelity resolution of vascular networks in live mice. Leveraging this imaging precision, the team could accurately identify thrombus sites and guide targeted photothermal ablation *in situ*. While these results underscore the potential of NIR-II imaging to integrate diagnosis with therapy, its effectiveness at greater tissue depths and overall translational robustness warrant further investigation.

NIR-II optical imaging can also be integrated with other imaging modalities to enhance diagnostic capabilities: photoacoustic imaging: the integration of NIR-II imaging with photoacoustic detection achieves high-resolution, high-contrast visualization of deep-seated tissues. Demonstrating this synergistic potential, Liu *et al.*[24] developed the cyanine-based dye A1094, which enabled accurate delineation of glioma boundaries. This work exemplifies how optical-acoustic synergy can enhance structural mapping beyond the depth and contrast limits of conventional fluorescence imaging. Magneto-optical imaging: the integration of NIR-II fluorescence with MRI enables the concurrent observation of anatomical structures and molecular-level changes. Li *et al.*[25] demonstrated this multimodal approach by developing ASA6 nanoparticles, which allowed non-invasive imaging of atherosclerotic plaques through both NIR-II fluorescence and MRI contrast. Although such a dual-readout strategy enhances diagnostic reliability, the interplay between nanoparticle loading, MRI relaxation efficacy, and fluorescence brightness requires systematic optimization to maximize the synergy of this combined modality. NIR-II/CT dual-modality imaging: the integration of NIR-II fluorescence with CT addresses the inherent depth limitations of purely optical methods by combining functional biological readouts with high-resolution anatomical context. This multimodal synergy provides enhanced spatiotemporal resolution, enabling detailed structural analysis alongside concurrent acquisition of dynamic physiological information. NIR-II/PET imaging: Hybrid imaging platforms that combine NIR-II fluorescence with PET enable precise tumor localization and guided surgical resection. As an example, Cheng *et al.*[26] developed a dual-modality nanotracer by integrating the NIR-II fluorophore CH-4T with the positron-emitting isotope ^{64}Cu, which simultaneously provides optical and nuclear signals for accurate intraoperative identification of tumor margins. For such integrated probes to advance toward clinical use, however, key practical factors including radiochemical stability and *in vivo* clearance kinetics must be systematically evaluated.

The development of NIR optical agents follows a clear evolutionary path, progressing from fundamental material innovation to sophisticated biomedical applications, and from passive imaging toward active theranostic platforms. This journey began in 1959 when the U.S. FDA approved ICG for clinical use.[27] This milestone validated the concept of superior tissue penetration by NIR-I photons and provided early proof-of-principle for the clinical translation of optical technologies. However, initial applications were limited by insufficient target specificity, which constrained diagnostic accuracy. Around the turn of the millennium, advances in chemical biology enabled the conjugation of NIR-I dye such as Cy5.5 with antibodies or peptides, giving rise to targeted molecular probes.[28] This transition represented a critical shift from nonspecific staining toward molecular-level recognition, enhancing both the SNR and the biological information content of optical images. Nevertheless, the inherent limitations of NIR-I imaging—notably its shallow penetration depth and moderate spatial resolution—soon became apparent. During the period from 2009 to 2012, the field strategically pivoted to the NIR-II window. Pioneering studies that utilized single-walled carbon nanotubes (SWCNTs) demonstrated that tissue scattering and autofluorescence are substantially suppressed within this spectral region, thereby enabling deeper *in vivo* penetration and higher-resolution imaging.[29] While these findings ushered in a new era for optical bioimaging, practical implementation of NIR-II technology continues to be shaped by persistent challenges in biocompatibility, probe standardization, and adaptation across diverse tissue types. To address these translational hurdles, water-soluble small-molecule NIR-II dyes such as CH1055 were subsequently developed in 2014. These dyes feature well-defined chemical structures, favorable biocompatibility, and rapid *in vivo* clearance, offering greater clinical potential compared with early nanomaterial-based systems.[30] With the continuous emergence of high-performance probes, the functionality of NIR optical agents has expanded beyond diagnostic imaging. Since the mid-2010s, the concept of ''theranostics'' has gained momentum. Researchers have ingeniously integrated imaging moieties (*e.g.*, ICG or NIR-II dyes) with therapeutic components (*e.g.*, photothermal or photosensitizing agents) into unified platforms such as liposomes and polymeric nanoparticles, achieving the innovative paradigm of ''seeing and treating simultaneously''.[31] Meanwhile, the introduction of aggregation-induced emission luminogens (AIEgens) provided a revolutionary solution to the intrinsic problem of aggregation-caused quenching (ACQ) observed in conventional fluorophores. Since 2015, NIR AIEgens have become ideal materials for constructing highly emissive and efficient phototheranostic agents, owing to their unique property of synergistically enhanced fluorescence and reactive oxygen species (ROS) generation in the aggregated state.[32] Entering the 2020s, the field has witnessed rapid and synergistic progress toward diversification and precision.[15] In imaging, NIR-II–guided precision surgery has demonstrated successful identification and resection of submillimeter-scale tumors in preclinical models, with exceptionally high SNR underscoring its significant clinical value.[33] Research frontiers have since extended to longer wavelengths. Around 2022, the introduction of the NIR-IIb subwindow (1500–1700 nm) enabled ultra-high-contrast visualization of deep-seated structures such as cerebral vasculature. By further suppressing photon scattering, this approach pushed the penetration limits of *in vivo* optical imaging to unprecedented levels.[34] In the past few years (2023–2024), transformative innovations have accelerated progress on two parallel fronts. One direction focuses on enhancing signal intensity: the development of ultrabright NIR-II probes—such as Tm^{3+}-doped lanthanide nanoprobes[35] and biomimetic protein-shell fluorescent proteins, alongside advances in AIEgens—has provided powerful tools for deeper and multiplexed functional imaging. The other direction prioritizes biological precision and clearance: a representative breakthrough was reported in 2024 with the design of ''protein-escape'' cyanine dyes.[36] Through subtle structural modifications, these dyes avoid nonspecific binding to serum albumin, thereby achieving high-contrast vascular imaging while enabling rapid systemic

clearance. This class of probes offers critical solutions for applications requiring real-time intraoperative guidance and longitudinal monitoring. In 2025, Wen *et al.*[37] reported a design strategy for NIR-II fluorophores characterized by unusually large Stokes shifts (167–260 nm in chloroform). A representative formulation, VIPI-4 liposomes, achieved high-resolution visualization of fine bone structures in the knee joints of female mice at wavelengths beyond 1300 nm. Beyond its practical imaging utility, the study provided fundamental insights into the excited-state photophysics governing the NIR-II window, thereby offering a rational design blueprint for long-wavelength, large-Stokes shift fluorophores. Over the past six decades, NIR optical agents have evolved from simple diagnostic dyes into multifunctional platforms that now support high-precision imaging, minimally invasive surgical guidance, targeted therapy, and immune modulation. Looking forward, deeper integration of chemistry, materials science, and biology is expected to yield activatable probes with higher specificity, advanced bioorthogonal labeling strategies, and broader clinical applicability. These advances are poised to further expand the frontiers of life science research and precision medicine (Fig. 2). Nevertheless, the translation of such innovations continues to face practical hurdles, including scalable probe manufacturing, long-term *in vivo* stability, and the establishment of regulatory-ready standardization frameworks.

Optical imaging in NIR-II window represents a transformative advance for biomedical imaging and precision diagnostics. The field has evolved from early dyes like ICG to sophisticated agents—including inorganic nanoparticles, organic fluorophores, and rare-earth-doped materials—progressively enhancing resolution, penetration depth, and real-time monitoring in living subjects. By overcoming key limitations of conventional modalities (*e.g.*, CT, MRI, PET, SPECT), NIR-II imaging enables non-invasive, high-sensitivity visualization of both structural and molecular dynamics. The development of multifunctional theranostic agents, which combine diagnosis, therapy, and surgical guidance, signals a shift toward integrated, intelligent medical platforms (Scheme 1). However, the clinical translation of NIR-II imaging remains hindered by several unresolved challenges, particularly in biosafety validation, imaging hardware performance, and clinical standardization. From a formulation-centered perspective, overcoming these barriers requires not only the rational engineering of biocompatible, biodegradable, and activatable optical agents with controllable pharmacokinetic and optical properties, but also improvements in detector sensitivity, manufacturing reproducibility, and regulatory evaluation frameworks. Looking forward, the integration of chemistry, materials science, bioengineering, and clinical medicine—together with advances in portable imaging systems and artificial intelligence-assisted image

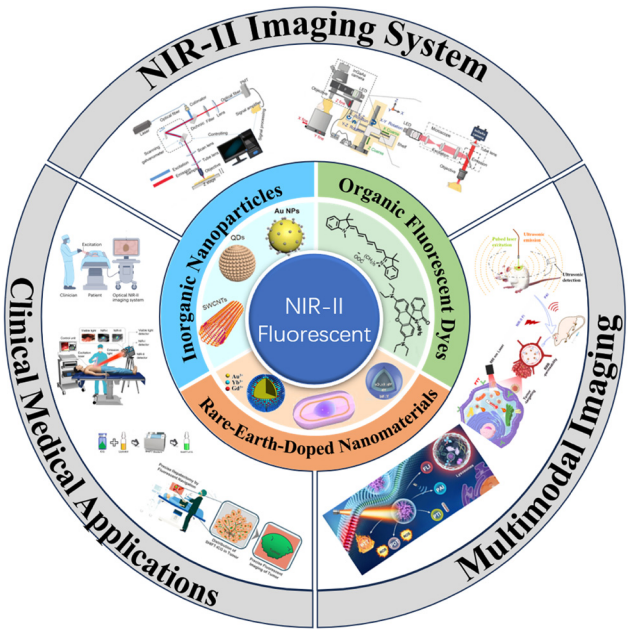

Scheme 1 Schematic diagram of NIR-II fluorescent classification. Combination image of clinical medical application, NIR-II imaging system and multimodal imaging. Copyright 2019, Springer Nature;[33] Copyright 2022, Oxford University press;[38] Copyright 2024, Springer Nature;[18] Copyright 2024, John Wiley and Sons;[39] Copyright 2020, American Chemical Society;[40] Copyright 2025, John Wiley and Sons;[41] Copyright 2021, Elsevier;[42] Copyright 1997, American Chemical Society;[43] Copyright 2025, Springer Nature;[44] Copyright 2016, Elsevier;[45] Copyright 2026, Elsevier.[46]

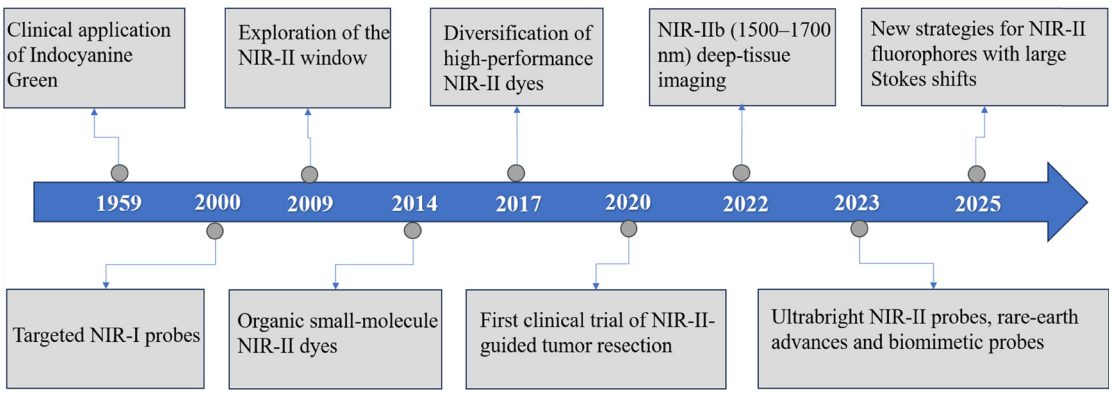

Fig. 2 Development of NIR optical agents.

analysis—is expected to accelerate the evolution of NIR-II technologies from signal-generating probes toward clinically actionable optical agents. Such interdisciplinary progress may ultimately position NIR-II imaging as a key enabling platform for precision diagnostics, image-guided interventions, and personalized medicine.

2. Classification of common NIR-II fluorescent probes

2.1 Organic fluorescent dyes

Based on differences in their chemical structures, currently reported NIR-II organic molecules can be classified into four main categories: small molecules containing the benzobisthiadiazole (BBTD) core, cyanine dyes, oxanthracene-based dyes, and Boron-dipyrromethene (BODIPY) derivatives.[47–49]

Small molecules based on BBTD typically adopt a donor–acceptor–donor (D–A–D) architecture and exhibit excellent photostability, broad emission spectra, and high molar extinction coefficients. In recent years, numerous studies have designed various NIR-II fluorophores by leveraging the unique structure of BBTD (Fig. 3a).[47,50,51] Cyanine dyes consist of a polymethine chain flanked by two terminal groups. Although these dyes often suffer from low quantum yields (QY, defined as the ratio of emitted photons to absorbed photons for evaluating fluorescence efficiency) and may be prone to photobleaching, they possess high extinction coefficients. Their optical performance can be enhanced by structural modifications, such as adjusting the length of the conjugated chain and introducing functional groups (Fig. 3b).[52] Previous investigations have demonstrated that the introduction of electron-withdrawing substituents, such as fluorine, together with sterically bulky groups can effectively reduce the electron density along the polymethine backbone. This strategy consequently suppresses the susceptibility of the backbone to oxidative C–C bond cleavage. Furthermore, a supramolecular strategy involving the encapsulation of polymethine dyes within a polymer matrix has been reported to enhance molecular rigidity. This approach can significantly improve the QY of these dyes.[53] Oxanthracene-based dyes, such as fluorescein, rhodamine, and their analogues, are characterized by high extinction coefficients, robust photostability, minimal cytotoxic effects, strong fluorescence efficiency, and readily adjustable emission wavelengths (Fig. 3c).[54] Although their excitation and emission wavelengths typically fall within the visible range, extending the π-conjugation of the chromophore can shift the emission into the NIR-I or even NIR-II window. For example, fusing naphthalene rings or styryl groups with the oxanthracene scaffold has led to the development of novel NIR-I/II emissive oxanthracene dyes.[55] Another widely adopted strategy for achieving NIR emission from oxanthracene derivatives involves replacing the central oxygen atom at the 10-position with other heteroatoms (*e.g.*, S, Se, P, Si, Ge, Sn, Te) or functional groups such as PO_2, POR, or SO_2.[54,56] BODIPY compounds have received broad attention due to their tunable fluorescence QY, excellent photostability, low toxicity, and high molar extinction coefficients. BODIPY derivatives have been extensively exploited across a broad range of applications, including biosensing, biological imaging, photodynamic and photothermal therapies, as well as solar energy harvesting

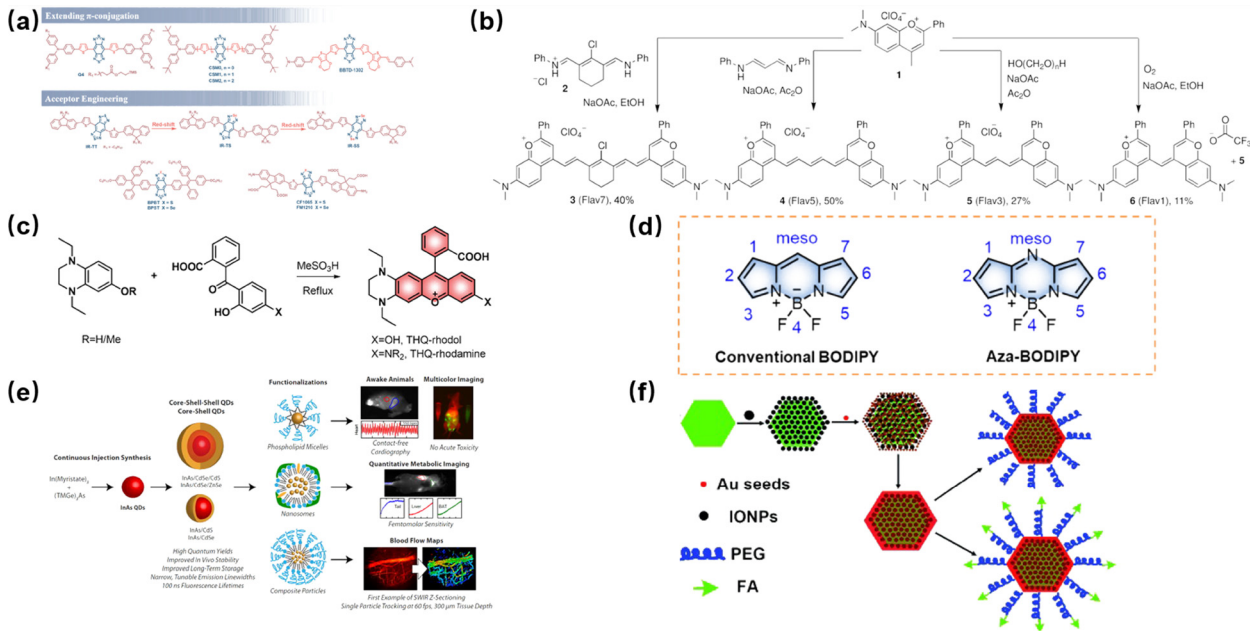

Fig. 3 (a) Chemical structures of BBT-based NIR-II dyes engineered *via* π-conjugation extension and acceptor modification. Copyright 2024, American Chemical Society.[47] (b) Synthesis of dimethylamino flavylium polymethine dyes 3–6. Copyright 2017, John Wiley and Sons.[52] (c) General synthetic route for THQ-xanthene. Copyright 2023, John Wiley and Sons.[54] (d) Structures of conventional BODIPY and Aza-BODIPY cores. Copyright 2022, Elsevier.[58] (e) Schematic of InAs-based core–shell and core–shell-shell SWIR QDs synthesis, shell engineering, and surface functionalization for imaging applications. Copyright 2017, Springer Nature.[15] (f) Strategy for MFNP synthesis and functionalization. Copyright 2011, John Wiley and Sons.[72]

(Fig. 3d).[57–59] It has been reported that the aqueous solubility of nitrogen-substituted BODIPY dyes can be substantially enhanced through the introduction of hydrophilic functionalities at the 2,6-positions of the BODIPY scaffold. In addition, ammonium groups can be introduced at the boron center to further improve water solubility. These modifications eliminate the need for additional hydrophilic coatings or PEG modification.[60] Owing to its intrinsically electron-deficient nature, the BODIPY core is commonly regarded as an acceptor unit, enabling the rational design of D–π–A–π–D conjugated systems when paired with electron-donating moieties. Such molecular engineering promotes efficient intramolecular charge transfer, ultimately supporting fluorescence emission within the NIR-II window.[61]

2.2 Inorganic nanoparticles

Common nanomaterials used in NIR-II fluorescent probes include quantum dots (QDs), gold nanoparticles (AuNPs), and carbon nanotubes (CNTs).

QDs are semiconductor nanocrystals, typically 2–10 nm in size, whose dimensions are smaller than twice the exciton Bohr radius of the corresponding bulk semiconductor material in all three spatial dimensions. Common QDs are composed of IV, II–VI, or III–V elements, such as silicon QDs, germanium QDs, cadmium selenide QDs, and indium phosphide QDs. Based on morphology, QDs can be further categorized into spherical, rod-shaped, cubic, and other complex-shaped structures. QDs possess outstanding optical properties, including broad absorption spectra, narrow emission peaks, tunable fluorescence, high QY, long fluorescence lifetimes, and excellent photostability. Bawendi *et al.*[15] employed high-quality indium arsenide-based QDs emitting in the SWIR region to concurrently measure lipoprotein metabolic turnover in multiple organs while monitoring cardiac and respiratory dynamics in freely moving, awake mice. This approach enabled the construction of a comprehensive three-dimensional, quantitative map of *in vivo* biodistribution (Fig. 3e). Wang *et al.*[62] were the first to demonstrate silver sulfide (Ag_2S) QDs exhibiting strong NIR-II fluorescence, synthesized *via* thermal decomposition of an Ag(DDTC) [$(C_2H_5)_2NCS_2Ag$] precursor. Building on this work, later studies achieved Ag_2S QDs with high optical quality, delivering QY of approximately 20% and emission wavelengths tunable from 900 to 1250 nm.[63,64] Notably, the absence of toxic heavy-metal elements endows Ag_2S QDs with favorable biocompatibility. Furthermore, surface functionalization can improve their aqueous dispersibility, making them particularly attractive for tumor imaging applications. AuNPs, although derived from one of the most chemically stable elements, exhibit unique optoelectronic and physicochemical properties at the nanoscale (1–100 nm), along with good biocompatibility. Compared with many other metallic nanomaterials, AuNPs exhibit superior biosafety. As a result, they have been widely utilized in biomedical applications ranging from rapid diagnostics to therapeutic interventions. For instance, Smedt *et al.*[65] reported that hyaluronic acid-coated AuNPs combined with ICG can spontaneously accumulate in vitreous haze within rabbit eyes. Upon exposure to nanosecond laser pulses, these complexes generate vapor nanobubbles capable of disrupting vitreous opacities noninvasively. While this strategy demonstrates potential for treating ocular haze, its clinical translation still requires careful evaluation. In particular, localized thermal effects and the reproducibility of nanobubble formation should be thoroughly investigated. CNTs, also known as buckytubes, represent another important class of nanomaterials. Structurally, they consist of one or more concentrically rolled graphene sheets forming seamless cylindrical nanostructures with hexagonal carbon lattices. Based on the number of graphene layers, CNTs are categorized as SWCNTs or multi-walled (MWCNTs). SWCNTs, typically with diameters below a few nanometers, exhibit exceptional physicochemical properties that make them attractive for deep-tissue fluorescence imaging. Surface functionalization further improves their biocompatibility, enables targeted therapeutic delivery, and facilitates integration with other imaging modalities for multimodal applications. Dai *et al.*[66] first employed PL-PEG-modified SWCNTs as NIR-II fluorescent probes for *in vivo* imaging. Expanding on this, Bhatia *et al.*[67] functionalized SWCNTs with M13 bacteriophages and targeting peptides, markedly improving aqueous dispersibility and enabling tumor visualization and treatment monitoring. Mukhopadhyay *et al.*[68] further demonstrated that DNA-wrapped SWCNTs implanted in pancreatic ductal adenocarcinoma (PDAC) models could dynamically report intratumoral hydrogen peroxide levels, providing a sensitive readout of chemotherapy efficacy. Beyond these strategies, CNT-based probes can be optimized *via* covalent or noncovalent surface engineering, including PEGylation or incorporation of carboxyl and amino groups, and through conjugation with peptides or antibodies for selective tumor targeting. Welsher and colleagues employed sodium cholate-assisted sonication followed by surfactant exchange to coat SWCNTs with PL-PEG, generating bright, biocompatible agents capable of high-resolution imaging of tumor vasculature *in vivo*. While these approaches demonstrate remarkable versatility, challenges related to long-term biocompatibility, reproducibility, and translational scalability remain to be addressed.

Nanomaterials—including QDs, AuNPs, and CNTs—are often engineered into NIR-II probes through surface functionalization and targeted modification. For instance, QDs can be encapsulated within biocompatible coatings such as PEG and further conjugated with targeting ligands (*e.g.*, antibodies or peptides). This design not only improves colloidal stability and targeting specificity but also extends circulation time *in vivo*, thereby enhancing overall imaging performance. Schipper *et al.*[69] conducted a systematic investigation into how QDs size, surface coating, and PEGylation influence their biodistribution in mice. Their study demonstrated that coatings such as PEG or specific peptides significantly delay clearance by the reticuloendothelial system (RES)—a critical factor for achieving stable and reproducible *in vivo* imaging. In a parallel strategy, AuNPs can be functionalized *via* thiol or amine groups and subsequently conjugated with biomolecules to achieve targeted delivery. When further integrated with fluorescent reporters, these functionalized AuNP clusters support multimodal imaging applications. NIR-II-

emissive gold nanoclusters modified with thiolated cyclodextrin (CD-Au NCs, emission at 1050 nm) were developed by Yang *et al.*[70] *In vivo*, these CD-Au NCs were shown to permit efficient tracking during blood circulation without impairing tumor targeting or altering biodistribution. Furthermore, strong stability under physiological conditions, efficient renal clearance, and good biocompatibility were demonstrated, highlighting their potential for sensitive tumor imaging. Although such nanomaterial-based NIR-II probes exhibit promising imaging performance, several challenges must be addressed before clinical translation can be realized. These include long-term biocompatibility, variability in RES-mediated clearance, and the need for reproducible, scalable synthesis.

In summary, the incorporation of nanomaterials into NIR-II fluorescent probes—through rational surface functionalization and targeted modification—significantly enhances diagnostic accuracy and imaging efficacy. These engineered probes provide a versatile platform for early disease detection and image-guided therapeutic interventions. Despite this promising outlook, the clinical translation of such probes requires systematic evaluation of key parameters, including long-term biocompatibility, *in vivo* stability, and overall feasibility for human use.

2.3 Rare-earth-doped nanomaterials

Rare-earth elements (REEs) comprise scandium, yttrium, and the 15 lanthanides from lanthanum to lutetium. These elements possess unique luminescent properties, including tunable emission, large Stokes shifts, and exceptional photostability. These features make them promising materials for bioimaging, sensing, anti-counterfeiting, and related technologies. To harness these optical properties in functional nanomaterials, rare-earth-doped nanoparticles (RENPs) are synthesized by incorporating RE ions into inorganic host crystal lattices. This approach yields nanostructures with precisely controlled optical characteristics, rendering them highly suitable for advanced imaging and diagnostic applications. Lanthanide ions (Ln^{3+}), owing to their rich energy level structures and multiple electronic transitions, endow RENPs with distinctive upconversion and downconversion luminescence characteristics.

Liu *et al.*[71] introduced a general design framework for $NaYF_4$-based rare-earth nanoprobes by employing a single host lattice co-doped with ytterbium (Yb^{3+}), thulium (Tm^{3+}), and erbium (Er^{3+}). Through precise regulation of lanthanide composition and dopant concentrations, this system enabled emission spanning from the visible to the NIR region under excitation at a single wavelength. Previous studies have reported the successful synthesis of lanthanide-functionalized AuNPs, which were effectively applied in *in vivo* MRI, CT imaging, and photothermal therapy (PTT) in tumor-bearing mice.[45] In another study, Liu *et al.*[72] constructed multifunctional UCNP–Fe_3O_4–Au nanocomposites that enabled dual-mode upconversion luminescence/MRI imaging as well as magnetically targeted PTT (Fig. 3f).

In terms of biosafety, key factors for evaluating RENPs include biocompatibility, cytotoxicity, degradability, and potential long-term effects. Ju *et al.*[73] summarized that lanthanide-doped RENPs emitting in the NIR-II window exhibit favorable biocompatibility, rendering them promising optical agents for early-stage disease detection and tumor treatment. From a translational perspective, the clinical adoption of RENPs depends on several practical factors. These include structural stability, batch-to-batch reproducibility, scalable synthesis, and consistent optical performance under physiological conditions. The significance of these properties is illustrated in a study where RENPs were engineered for high-precision photoluminescence-based nanothermometry, demonstrating their potential for *in vivo* temperature sensing and related diagnostic applications.[47] Despite such promising functional demonstrations, key translational hurdles remain—particularly concerning the long-term stability of RENPs in complex biological milieus and the scalability of their manufacturing processes to clinically relevant quantities.

In conclusion, RENPs present a promising clinical outlook due to their favorable biosafety and multifunctional capabilities. However, their translation necessitates thorough *in vivo* validation and rigorous assessment of long-term safety and efficacy. Continuous research efforts are expected to address these requirements, thereby facilitating the future integration of RENPs into clinical practice. Conversely, the clinical application of many inorganic phototheranostic agents is hindered by inherent limitations, such as poor biodegradability and relatively low photothermal conversion efficiency (PCE), which pose significant challenges for their practical use. In contrast, organic phototheranostic agents demonstrate significant potential in tumor phototherapy owing to their superior biocompatibility and strong NIR absorption properties. However, the PCE of currently reported organic phototheranostic materials remains relatively low. In particular, multifunctional agents that integrate both imaging and therapeutic capabilities within the NIR-II window are still scarce, which has severely hindered the further clinical translation of phototheranostic approaches.

3. From optical probes to translational optical agents

3.1 Limitations of standalone optical probes for clinical translation

Although numerous NIR-II probes exhibit excellent optical responsiveness and imaging capability under experimental conditions, most standalone probes remain insufficiently equipped for direct biomedical and clinical translation. In practical physiological environments, successful *in vivo* applications require not only intrinsic optical performance, but also systemic properties including physiological stability, biosafety, controllable pharmacokinetics, prolonged circulation, efficient clearance, and target specificity. However, these translational requirements are difficult to achieve using unmodified probes alone.

Among currently reported systems, inorganic nanoparticles generally possess superior photostability and high fluorescence brightness, yet their clinical applicability is frequently restricted by biosafety concerns. Many inorganic probes, including QDs and RENPs, contain heavy-metal or non-biodegradable

components that tend to accumulate in organs such as the liver and spleen after systemic administration, thereby increasing the risk of long-term toxicity (Fig. 4a).[74,75] In addition, most inorganic nanoparticles exhibit relatively large hydrodynamic diameters (>10 nm), making them susceptible to macrophage uptake and reticuloendothelial system sequestration during circulation, while simultaneously limiting rapid renal clearance and increasing nonspecific biodistribution. These characteristics substantially hinder their translational potential despite their favorable optical properties.

In contrast, organic fluorophores generally display lower intrinsic toxicity and improved structural tunability, making them attractive candidates for clinical translation. Nevertheless, many NIR-II organic dyes still suffer from inadequate aqueous dispersibility, poor photostability, ACQ, and insufficient QY under physiological conditions. Most reported small-molecule fluorophores possess highly conjugated hydrophobic frameworks and molecular weights frequently exceeding 500 Da, which complicates direct *in vivo* administration and limits systemic stability. Furthermore, the fluorescence performance of many organic probes deteriorates substantially in complex biological microenvironments, thereby restricting imaging sensitivity and long-term applicability.

RENPs provide additional advantages including long luminescence lifetimes, narrow emission bands, and excellent resistance to photobleaching. However, their intrinsically low absorption cross-sections and limited excitation efficiencies often require high-power laser excitation or sensitization strategies to achieve sufficient signal intensity. More importantly, RENPs themselves remain poorly biodegradable and generally require extensive surface engineering, such as PEGylation or biomembrane coating, to improve colloidal stability, hydrophilicity, circulation behavior, and *in vivo* compatibility. Without appropriate formulation optimization, these systems also exhibit substantial hepatic and splenic accumulation after administration.

Collectively, these limitations indicate that most NIR-II probes primarily function as optical signal-generating materials rather than clinically applicable biomedical systems. While probes provide intrinsic fluorescence or photoacoustic functionality, they alone are typically unable to satisfy the complex physiological and translational requirements necessary for *in vivo* applications. Therefore, substantial formulation engineering—including surface functionalization, hydrophilic modification, size optimization, targeting integration, and carrier-assisted assembly—is essential for transforming optical probes into translational optical agents suitable for biomedical and clinical use. This probe-to-agent transition has consequently become a central direction in the development of next-generation NIR-II imaging systems.

3.2 Formulation engineering strategies for optical agent construction

3.2.1 Targeting engineering. To increase probe accumulation in tumors or other lesions, investigators typically conjugate

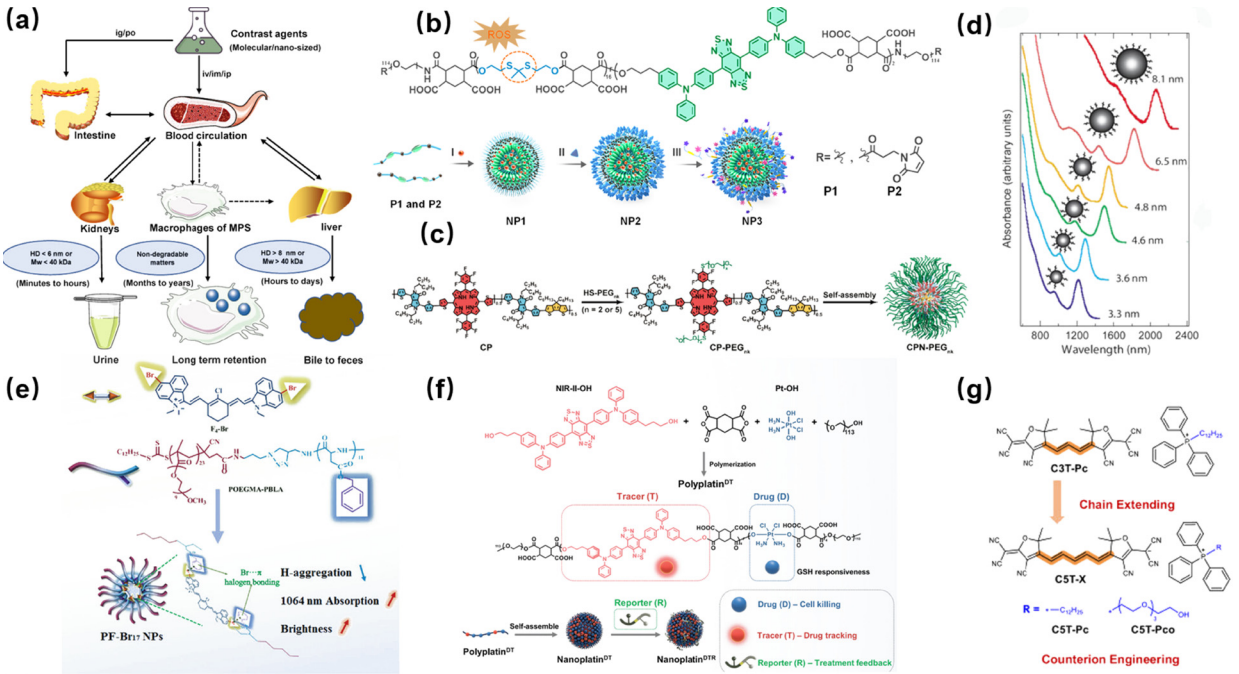

Fig. 4 (a) Clearance pathways of contrast agents. Copyright 2026, Ivyspring International Publisher.[92] (b) Design of a NIR-II fluorescent biodegradable polymer for drug delivery and bioimaging on a multi-drug resistant lung cancer PDX^{MDR} model. Copyright 2021, American Chemical Society.[77] (c) Schematic representation of the construction of CPN-PEGnk. Copyright 2026, Ivyspring International Publisher.[78] (d) Size-dependent absorption spectra of QDs reveal a quantum confinement-induced shift in the first excitonic absorption peak. Copyright 2023, American Chemical Society.[98] (e) Illustration of the development of bright NIR-II fluorescent nanoprobe F4-Br@P17. Copyright 2023, John Wiley and Sons.[88] (f) Illustration of NIR-II fluorescent Nanoplatin^{DTR} theranostic platform. Copyright 2024, John Wiley and Sons.[95] (g) Molecular structure of anionic cyanines C3T-Pc, C5T-Pc and C5T-Pco. Copyright 2025, Springer Nature.[96]

targeting ligands to NIR-II probes to direct them to specific receptors or organelles. Common targeting ligands include integrin ligands (*e.g.*, RGD peptides), blood–brain-barrier penetrating peptides (*e.g.*, lactoferrin), and mitochondria-targeting triphenylphosphonium (TPP). For example, Hong *et al.*[76] linked a TPP carboxyl group to the NIR-II blinking dye H4 *via* a PEG spacer to form the H4-PEG-TP probe. This probe rapidly accumulated in osteosarcoma cell mitochondria, enabling subcellular localization imaging while providing high SNR tumor imaging and excellent photothermal performance. Xiao *et al.*[77] engineered a degradable conjugated polymer system in which NIR-II-emissive fluorophores were incorporated directly into the polymer backbone, while RGD targeting ligands and a cisplatin-derived anticancer agent (56MESS) were covalently attached. The self-assembled nanoparticles, with an average diameter of ∼100 nm, enabled high-contrast *in vivo* NIR-II tumor visualization and simultaneously supported on-site drug release with real-time monitoring of therapeutic responses (Fig. 4b). In addition, activatable NIR-II agents that respond to pathological proteolysis, acidic microenvironments, or ROS can indirectly achieve lesion specificity (Fig. 4c).[78] In summary, decorating probes with targeting peptides, receptor ligands, or other targeting moieties effectively enhances tumor or vascular localization (Table 1).

3.2.2 Hydrophilicity engineering. Neat NIR-II dyes synthesized chemically are typically hydrophobic and poorly dispersible in biological media. To improve water solubility and biocompatibility, strategies such as PEGylation, polymer encapsulation, water-soluble ligands, or liposomal formulations are commonly employed. For example, Zheng *et al.* prepared a PEGylated conjugated polymer probe (CPN-PEG_5k); compared with an F127-encapsulated control, PEG modification increased NIR-II fluorescence intensity by nearly threefold while retaining up to 58.6% photothermal conversion efficiency. This probe produced high-definition vascular imaging in mouse circulation with a SNR of 8.9 and effectively suppressed tumor growth.[91] Introducing hydrophilic groups into nanoparticle systems can also prevent probe aggregation and preserve high QY. Yan *et al.* reported an amphiphilic peptide polymer that co-loads hydrophilic chains and hydrophobic NIR-II dyes, which significantly suppresses H-type aggregation of the dyes and markedly enhances fluorescence brightness in aqueous phase; the nanoparticles demonstrated high resolution and high contrast in *in vivo* vascular microscopy (Fig. 4e).[88] In general, hydrophilic polymers (such as PEG) reduce protein adsorption and mononuclear phagocyte system (MPS) clearance, thereby prolonging blood half-life. Probes surface-modified with hydrophilic polymers are more stable in blood and more amenable to renal clearance than hydrophobic

Table 1 Quantitative comparison of representative formulation-engineered NIR-II optical agents and their translational performance

Representative agent	Formulation strategy	Size (nm)	Circulation half-life	Major clearance pathway	Renal excretion	SNR improvement	Ref.
Nanoemulsion	Self-emulsifying nanotechnology	∼100 nm	NA	Hepatobiliary clearance	Minimal renal clearance	5-fold	79
SHIFT ICG	super-stable homogeneous intermix formulating technology	NA	NA	Hepatobiliary clearance	Minimal renal clearance	∼1.8-fold *vs.* conventional ICG	80 and 81
LZ-1105	Long-circulation molecular engineering	∼3–4 nm	3.2 h	Renal clearance	86% ID excreted in urine within 24 h	11.3-fold signal enhancement in urine	82
PSO	PEGylation/hydrophilic engineering	5 nm	∼1.8 h	Renal clearance	Partial renal clearance observed within 24 h	∼3-fold higher tumor fluorescence intensity than non-PEGylated control	83
β-LG@IR-780	Protein-assisted assembly	4.1 nm	∼2 h	Renal clearance	∼75% ID renal clearance within 24 h	5.6-fold higher vascular SNR than free dye	84
LUM015	PEGylation/hydrophilic engineering	NA	NA	Renal clearance	Partial renal clearance; uncleaved probe detected in kidney	4.1	85
GE-137	Targeting engineering	NA	NA	Renal clearance	0.13 kg^{-1} h^{-1}	Tumor to muscle ratio ≈ 12	86
DCNPs@ Si-omSi RGD	Targeting engineering	255 nm	NA	Hepatobiliary clearance	NA	SNR ≈ 15 after tail vein injection for 48 h	87
F4-Br@P17 nanoparticles	Molecular engineering	31 nm	NA	Hepatobiliary clearance	NA	SNR ≈ 12 for F4-Br@P17 nanoparticles VS SNR < 2 for ICG when depth comes to 6 mm	88
Fe-CPNDs	Size minimization engineering	5.3 nm	0.25 ± 0.04 h	Renal clearance	65% ID excreted in urine within 24 h	NA	89
TCPP-PEG_{10K}	PEGylation/hydrophilic engineering	14.2 ± 2.8 nm	17.62 ± 3.34 min	Renal clearance	40.05 ± 8.70 min	NA	90

Abbreviations: ID, injected dose; SNR, signal-to-noise ratio; NA, not available.

probes, reducing nonspecific accumulation. Therefore, conjugating NIR-II fluorophores to PEG, starch, proteins, or other water-soluble carriers can improve plasma stability and distribution homogeneity, making probes better suited for *in vivo* vascular and tumor imaging applications.

3.2.3 Size engineering. The nanoscale size of a probe directly influences *in vivo* distribution, tumor penetration, and clearance route. Generally, ultrasmall probes (<6–8 nm or molecular weight <40 kDa) can be rapidly filtered by the glomerulus for renal clearance, whereas nanoparticles larger than ~8–10 nm more commonly rely on the mononuclear phagocyte system and hepatobiliary metabolism.[92] Therefore, controlling probe size enables a balance between rapid clearance and high accumulation. Tumor penetration: smaller probes more readily penetrate the tumor stroma and rapidly contact tumor cells. For instance, tumor microenvironment-responsive degradable silica nanoplatforms have been engineered to undergo framework decomposition under pathological conditions, leading to activatable fluorescence recovery and enhanced signal specificity at diseased tissues.[93] Conversely, overly large particles are difficult to extravasate and carry increased risk of long-term retention *in vivo*. Large nanoparticles readily accumulate in the liver and spleen, potentially causing toxicity; thus, rational control of particle size (*e.g.*, ~10–100 nm) favors tumor enrichment while allowing controllable clearance. In summary, probe design should consider size effects on biodistribution and clearance: ultrasmall probes tend toward rapid circulation and excretion, whereas mid-sized probes can exploit the enhanced permeability and retention (EPR, refers to the preferential accumulation of nanomaterials in tumor tissues owing to leaky vasculature and poor lymphatic drainage) effect for tumor imaging.[94]

3.2.4 Carrier-assisted drug integration. Incorporating therapeutic agents into NIR-II optical probes enables integrated imaging-and-therapy (''photothermal/photochemical therapy + chemotherapy''). Common strategies involve covalent or non-covalent loading of anticancer drugs onto probe carriers. For example, Xiao *et al.* conjugated NIR-II fluorophores and a platinum-based drug (56MESS) onto a degradable polymer chain to form self-assembling nanoparticles. These particles are taken up *via* RGD targeting and synchronously release drug payloads *in vivo*; researchers directly observed quantitative drug release within deep tumors by laser desorption mass spectrometry (Fig. 4b).[77] Xiao *et al.* further introduced the first ''Polyplatin'' polymeric platform, in which an NIR-II fluorescent reporter (T) and a Pt(IV) prodrug (D) were covalently incorporated into the polymer backbone at predetermined molar ratios. The engineered polymer spontaneously assembled into nanoscale particles (Nanoplatin^{DT}) and was subsequently functionalized with a caspase-responsive, apoptosis-sensing peptide to yield Nanoplatin^{DTR}. By ensuring co-transport of the therapeutic agent and fluorescent signal at a fixed stoichiometry, this system enabled real-time NIR-II visualization of platinum drug distribution alongside *in situ* reporting of apoptosis throughout the treatment process (Fig. 4f).[95] Collectively, these findings suggest that the direct integration of therapeutic agents into imaging probes or delivery platforms enables near-real-time drug tracking and imaging-assisted treatment, thereby substantially enhancing targeting precision and improving the reliability of therapeutic outcome assessment.

3.2.5 Other formulation optimization strategies. Beyond the above conventional strategies, structural optimization can enhance probe stability and signal intensity. For example, designing anti-aggregation motifs increases fluorescence QY and resistance to quenching. Li *et al.* reported an anionic cyano-dimethyl-tolyl dye (C5T) whose amphiphilicity was optimized by pairing it with a PEGylated triphenylphosphonium cation, effectively suppressing dye aggregation. This approach allowed the assembly to produce efficient type-I ROS under 760 nm excitation while maintaining strong NIR-II fluorescence under 808 nm excitation. This ''ionic engineering'' successfully achieved a dynamic balance between fluorescence imaging and photodynamic therapy, effectively enhancing signal and stability (Fig. 4g).[96] Additionally, AIE, J-aggregation engineering, and incorporation of rigid conjugated backbones can enhance NIR-II emission and QY. Lu *et al.*[97] demonstrated that AIE-active NIR-II nanoparticles based on BPBBT maintained stable fluorescence output during prolonged irradiation owing to restricted intramolecular motion and aggregation-enhanced photophysical robustness. Overall, combining the optimization routes above (optimizing aggregation-state optics, enhancing chemical stability, mitigating photobleaching, *etc.*) can significantly improve NIR-II probe imaging quality and biological applicability, offering superior solutions for tumor vasculature and deep-tissue *in vivo* imaging.

4. Preclinical and clinical applications by disease area

4.1 Cardiovascular and vascular applications

Cardiovascular and vascular diseases remain leading causes of morbidity and mortality worldwide, creating an urgent need for imaging modalities.[99] NIR-II fluorescence imaging significantly reduces tissue scattering and autofluorescence, thereby enabling superior SNR, enhanced penetration depth, and improved spatiotemporal resolution for vascular visualization. These advantages have promoted the rapid development of NIR-II optical agents for cardiovascular and vascular applications, particularly in angiography, thrombosis detection, ischemia monitoring, and atherosclerotic plaque imaging.

One of the earliest and most representative demonstrations of NIR-II vascular imaging was reported by Dai *et al.*, who employed SWNTs as NIR-II fluorophores for real-time visualization of mouse hindlimb vasculature.[100] The study achieved spatial resolution of approximately 30 μm and temporal resolution below 200 ms per frame at imaging depths of 1–3 mm, outperforming conventional NIR-I imaging and micro-CT. Importantly, NIR-II imaging enabled clear differentiation between arteries and veins based on distinct hemodynamic behaviors and allowed accurate quantification of blood flow velocity in ischemic femoral arteries. These findings

highlighted the unique capability of NIR-II imaging for dynamic vascular functional assessment.

Beyond anatomical angiography, NIR-II optical agents have shown substantial promise in thrombosis imaging. Early detection of arterial and venous thrombi is clinically crucial because therapeutic efficacy is strongly time-dependent. Conventional modalities such as CT, MRI, and ultrasound primarily visualize secondary structural changes rather than directly identifying fresh thrombi. In contrast, targeted NIR-II fluorescence agents can provide real-time visualization of thrombotic lesions with high sensitivity. Wu *et al.*[101] developed an RGD-modified NIR-II fluorophore agent (TTQ-PEG-c(RGD)) with high fluorescence stability and strong affinity toward activated platelets, enabling specific accumulation at thrombotic sites *in vivo*. The agent exhibited significantly enhanced NIR-II fluorescence signals at fresh thrombi, reaching peak intensity at 4 h post-injection, while competitive inhibition experiments further confirmed its integrin-targeting specificity. Importantly, TTQ-PEG-c(RGD) demonstrated the capability to distinguish fresh thrombi from old thrombi, highlighting its potential for early noninvasive thrombosis diagnosis.

NIR-II imaging has also demonstrated important potential in ischemia-related vascular disorders. Dynamic contrast-enhanced NIR-II imaging enables quantitative monitoring of blood perfusion, vascular remodeling, and collateral vessel formation in ischemic tissues. Hong *et al.*[102] demonstrated that NIR-II fluorescence imaging enabled high-resolution visualization of hindlimb vasculature and quantitative monitoring of tissue perfusion recovery in peripheral arterial disease models, highlighting its potential for dynamic ischemia monitoring and vascular functional assessment.

In atherosclerosis research, NIR-II optical agents are increasingly being explored for molecular imaging of vulnerable plaques. Zhang *et al.*[103] developed a neutrophil membrane-camouflaged NIR-II agent (Neu-NPs) for targeted imaging of inflamed, high-risk atherosclerotic plaques (Fig. 5a). Owing to the specific interaction between LFA-1 and ICAM-1, Neu-NPs achieved enhanced accumulation within inflammatory plaques in both ApoE−/− mice and rabbit atherosclerosis models, enabling sensitive visualization of vulnerable plaques and dynamic evaluation of plaque inflammation following treatment.

Recent advances in fluorophore engineering have further accelerated the translational potential of NIR-II vascular imaging. Organic small-molecule dyes, AIEgens, RENPs, and QDs have been optimized to achieve higher QY, longer blood circulation times, and improved biosafety profiles. Surface modification strategies such as PEGylation and biomimetic coating have additionally enhanced vascular retention and reduced nonspecific uptake by the reticuloendothelial system.

Despite these advances, several challenges continue to hinder the clinical translation of NIR-II optical agents in cardiovascular applications. Many inorganic fluorophores still face concerns regarding long-term biosafety, biodegradability, and clearance pathways. In addition, limited targeting specificity and insufficient fluorescence brightness in deep tissues remain obstacles for imaging small or early-stage vascular lesions. Standardization of imaging instrumentation, fluorophore synthesis, and quantitative imaging protocols will therefore

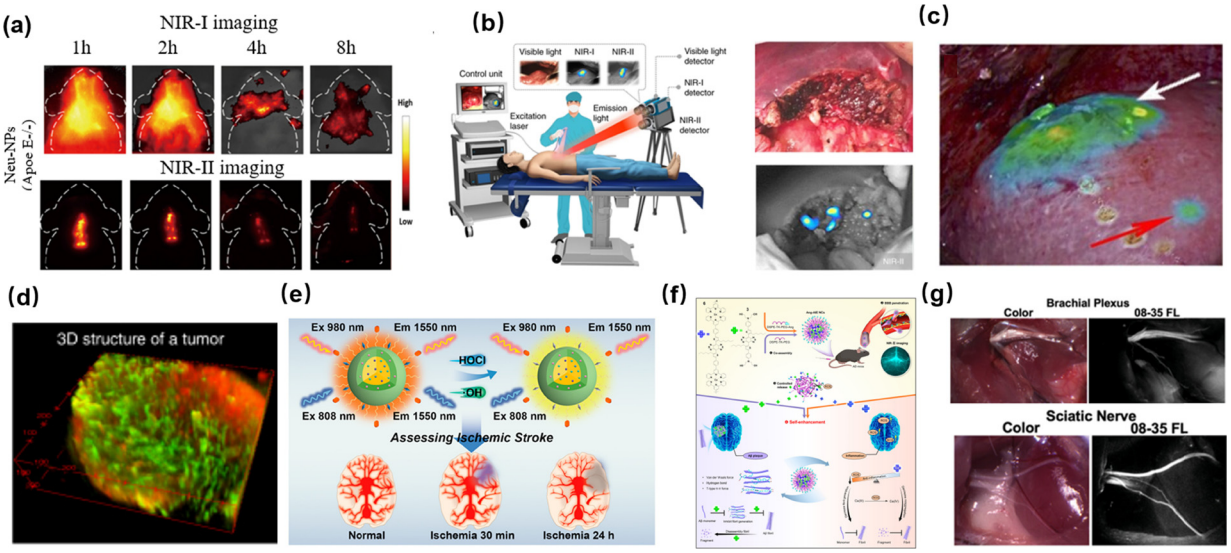

Fig. 5 (a) *In vivo* NIR-I and NIR-II fluorescence imaging at 1, 2, 4, and 8 h after intravenous injection (scale bar = 10 mm). Copyright 2022, Elsevier.[103] (b) In a representative patient with HCC, NIR-II imaging revealed residual fluorescence signals despite apparently complete tumor resection. Copyright 2019, Springer Nature.[33] (c) SHIFT-ICG fluorescence imaging guides surgery, revealing primary and metastatic tumors pre-resection *via* MRI correlation. Copyright 2022, Oxford University press.[38] (d) Confocal imaging of a tumor using two colors in the NIR-II window. Copyright 2018, Springer Nature.[114] (e) Ratiometric NIR-II luminescent nanoprobe enables assess ischemic stroke. Copyright 2021, American Chemical Society.[117] (f) Schematic of a NIR-II brain-targeted theranostic system enabling dual-target therapy for AD through a four-step pathway. Copyright 2024, Springer Nature.[121] (g) Representative images of rat brachial plexus and sciatic nerves following systemic administration of micelle-formulated LGW08-35. Copyright 2023, John Wiley and Sons.[125]

be essential for future clinical implementation. Nevertheless, with ongoing improvements in probe engineering and imaging hardware, NIR-II optical agents are expected to become increasingly important tools for precision cardiovascular diagnosis and intraoperative vascular guidance.

2.2 Cancer applications

Fluorescent agents can be employed to detect and analyze biomarkers such as proteins, nucleic acids, and organelles. For instance, fluorescent agents can quantitatively detect tumor markers, facilitating early diagnosis and monitoring of cancer therapy. PDAC is a highly fibrotic cancer with a five-year survival rate of less than 8%.[104] Combination therapies such as gemcitabine with nab-paclitaxel[105] or the FOLFIRINOX regimen[106] are the only first-line treatment options for PDAC. However, a major clinical challenge in chemotherapy is the lack of real-time therapeutic monitoring. To address this issue, Song *et al.*[107] developed a NIR-II fluorescent activatable drug-delivery nanoplatform capable of dynamically visualizing responsive drug release *in vivo*, thereby enabling real-time evaluation of tumor therapeutic responses during combined cancer therapy.

As a rapidly emerging and evolving biomedical imaging technique, NIR-II window fluorescence imaging has been the focus of extensive research in recent years. Wu *et al.*[108] developed an NIR-II fluorescent agent, CH1055-PEG-PT, incorporating an osteocalcin-mimetic peptide that exhibited strong binding affinity toward osteosarcoma cells. In noninvasive NIR-II imaging studies, this agent enabled visualization of osteosarcoma lesions smaller than 1 mm, which were not detectable by conventional CT. Moreover, CH1055-PEG-PT-assisted surgical navigation allowed complete excision of malignant tissue during osteosarcoma resection procedures. Other studies have reported the use of NIR-II optical agents for visualizing occult lesions in various organs, including micrometastases in the liver and lungs,[109] abdominal metastases of ovarian cancer,[110] and lymph node metastases in breast cancer.[111]

The first clinical investigation of NIR-II fluorescence-guided surgery (FMI) was reported in 2020, enrolling 23 patients diagnosed with hepatocellular carcinoma (HCC).[33] A multispectral imaging platform incorporating visible, NIR-I, and NIR-II channels was employed, with ICG serving as the contrast agent for both NIR modalities. The clinical outcomes validated the feasibility of NIR-II FMI and further demonstrated its superior tumor detection capability. Compared with NIR-I-guided surgery, NIR-II imaging achieved markedly higher sensitivity (100% *vs.* 90.6%) and diagnostic accuracy (91.4% *vs.* 82.9%). Importantly, NIR-II imaging uncovered five occult lesions that were missed preoperatively, whereas NIR-I detected only two of these lesions (Fig. 5b). In a related advancement, Li *et al.*[112] developed high-intensity NIR-II fluorescent polymer dots (NIR-II Pdots) for real-time visualization of metastatic ovarian cancer. Under NIR-II fluorescence guidance, metastatic nodules as small as 2 mm could be readily identified and surgically excised, highlighting the potential of NIR-II probes for precision oncologic surgery.

In 2023, Liu *et al.*[38] reported the successful application of a super-stable homogeneous intermixed formulation technology (SHIFT) for precision conversion hepatectomy in ruptured hepatocellular carcinoma. One patient with ruptured HCC received a combined treatment of embolization and fluorescence-guided surgery, showing excellent hemostatic effects. Both Lipiodol and ICG were effectively deposited in the primary lesion, and during subsequent laparoscopic liver resection, SHIFT-ICG provided clear and precise real-time imaging of the complete tumor region and boundaries (Fig. 5c). Even difficult-to-distinguish satellite lesions exhibited strong fluorescence intensity. This study suggests that the simple and environmentally friendly SHIFT-ICG formulation can be effectively used for emergency embolization and hemostasis in ruptured HCC patients, as well as for subsequent fluorescence-guided precision resection, offering significant clinical value.

Real-time vascular imaging provides both anatomical and hemodynamic information, which significantly enhances the accuracy of cancer detection and evaluation of therapeutic efficacy.[113] Dai *et al.*[114] developed an ultra-bright NIR-II complex, p-FE, by combining hydrophobic dyes with amphiphilic polymers (PS-PEG). Using a custom-built NIR-II confocal system, they performed three-dimensional vascular imaging in the mouse brain. Thanks to the high brightness of the fluorophore and the deep tissue penetration of NIR-II imaging, they achieved unprecedented 3D vascular imaging with single-photon NIR-II technology. Tiny vessels as narrow as 5–7 μm were visualized with high contrast at imaging depths reaching up to 1.3 mm (Fig. 5d).

NIR-II fluorescence imaging has established itself as a powerful tool for improving disease detection and guiding surgical procedures in both preclinical research and clinical practice. Compared to conventional radiological methods, it offers enhanced safety and superior spatial resolution.[115,116] This advantage stems from the intrinsic optical properties of NIR-II light: reduced tissue scattering and absorption enable greater penetration depth while delivering higher image contrast and resolution. Consequently, anatomical structures and pathological lesions can be visualized with greater precision. Furthermore, the significant suppression of background autofluorescence in this spectral window results in exceptionally clear images. Furthermore, it can be integrated with other imaging modalities, such as photoacoustic and MRI, to enable multimodal imaging, thus supporting more comprehensive diagnostic and therapeutic strategies.

4.3 Neurological and brain applications

Brain disorders represent a growing global health challenge, underscoring an urgent need for more effective diagnostic and therapeutic approaches. Despite significant advances, the development of noninvasive yet highly sensitive methods for neurological conditions remains a formidable task. Addressing this gap, Liu *et al.*[117] designed a ratiometric NIR-II agent responsive to ROS. Engineered through a dye-sensitized architecture that conjugates IR-783 with lanthanide-doped nanoparticles, this agent demonstrated the potential for real-time

in vivo monitoring of oxidative stress. This agent enabled discrimination between salvageable ischemic penumbra and infarct core in stroke models by visualizing agent accumulation at lesion sites, while simultaneously allowing ischemic tissue stratification through quantitative assessment of oxidative stress levels (Fig. 5e). Remarkably, NIR-II luminescence imaging delineated ischemic regions as early as 30 min after onset-substantially earlier than MRI-thereby offering a practical and timely strategy for acute ischemic stroke evaluation.

In 2022, Miao *et al.*[118] developed an NIR-II agent for the specific detection of Aβ plaques in Alzheimer's disease (AD) model mice. This agent demonstrated excellent blood–brain barrier (BBB) permeability and deep tissue penetration due to NIR-II fluorescence. It exhibited the highest affinity for Aβ fibrils, enabling specific detection of Aβ plaques in AD models. This work offered a promising strategy for non-invasive Aβ plaque imaging and a deeper understanding of AD progression. That same year, Han *et al.*[119] reported a family of NIR-II agent based on boron difluoride formazanate scaffolds that enabled noninvasive brain imaging by penetrating the BBB. In murine glioblastoma models, these agents effectively distinguished malignant lesions from surrounding healthy brain tissue. In 2024, Zhang *et al.*[120] proposed an innovative fluorescence quenching strategy based on a sterically hindered quencher (SHQ) that modulates molecular aggregation to suppress emission. Building on this concept, they established an ''off–on'' activatable sensing paradigm in which specific biological analytes deactivate the quenching function of SHQ. Using a hypochlorite (ClO^-)–responsive SHQ system, intense NIR-II fluorescence was generated in the hippocampus and in highly scattering brain tissues beneath the skull of epileptic mice, enabling real-time *in vivo* imaging of ClO^- production. In a related advance, Tang *et al.*[121] developed an NIR-II AIE nanoparticle-based therapeutic platform for the targeted treatment of Alzheimer's disease (Fig. 5f). Upon stimulation by ROS, two encapsulated AIE therapeutics were sequentially released to trigger a self-reinforcing treatment cascade. One agent selectively blocked amyloid-β fibrillogenesis, promoted fibril degradation, and inhibited re-aggregation, thereby alleviating inflammatory responses. The second agent efficiently scavenged excess ROS and further suppressed neuroinflammation, contributing to redox homeostasis restoration in the brain. Collectively, this approach mitigated neurotoxicity and produced marked improvements in behavioral and cognitive performance in female AD mouse models.

Among various anatomical targets, nerves are particularly difficult to visualize, making nerve imaging considerably more challenging. Earlier studies showed that *in vivo* NIR-I fluorescence imaging using ICG enables visualization of thoracic sympathetic nerves during thoracoscopic procedures as well as pelvic nerves in the context of radical hysterectomy.[122,123] However, NIR-II window imaging offers significant advantages in the field of nerve imaging. Under NIR-II imaging, ICG-labeled pelvic autonomic nerves can be identified more clearly, although the specificity of the imaging was lower than expected.[124]

Gibbs and colleagues[125] developed a nerve-specific near-infrared fluorescent contrast agent, LGW08-35, which was successfully used to image pelvic nerve anatomy in female rats and pigs. This work supports ongoing clinical translation and the potential for real-time identification of critical nerves such as the femoral, sciatic, lumbar, iliac, and hypogastric nerves (Fig. 5g). Further research on this contrast agent may help reduce nerve injury during gynecological surgeries. Wo *et al.*[126] reported an *in vivo* and *in situ* real-time imaging method based on NIR-II fluorescence for peripheral nerve visualization. This technique utilized PbS QDs that specifically bind to motor neuron-associated lectin proteins, allowing for clear imaging of peripheral nerve structures and potential damage in mouse models. This approach presents a promising strategy for the early diagnosis and precise treatment of peripheral neuropathies.

5. Multimodal imaging strategies based on NIR-II optical agents

Multimodal imaging refers to the integration of two or more imaging modalities within a single system to acquire more detailed diagnostic information than any individual modality alone can provide. Although each imaging technique has its own limitations-such as insufficient sensitivity or resolutionthey also possess unique advantages that can complement each other.[127] NIR-II imaging has demonstrated numerous strengths, and exploring strategies that combine it with other imaging modalities is crucial for improving clinical outcomes.

5.1 NIR-II imaging combined with MRI

MRI is a medical imaging technique based on the principles of nuclear magnetic resonance. It uses strong magnetic fields and radiofrequency pulses to excite hydrogen nuclei (protons) within the human body. When protons relax back to their original energy states, they emit radiofrequency signals that are detected and reconstructed to generate high-resolution images. This fundamental process enables MRI to provide detailed, non-invasive visualization of internal anatomy, including soft tissues, organs, blood vessels, and bony structures. Although MRI is costly and time-consuming, it is widely used in clinical settings due to its excellent soft tissue contrast and unrestricted penetration depth.

The combination of NIR-II imaging with MRI in dual-modality systems has shown great potential in the management and treatment of cancer patients. Cheng *et al.*[128] reported a tumor microenvironment-responsive, degradable silica-based nanoplatform that exploits the hydrogen peroxide-to-glutathione ratio for MRI and self-amplified chemodynamic therapy. Within this framework, NIR-II fluorescence imaging was applied to assess therapeutic target expression and to track drug delivery and intratumoral accumulation, whereas MRI provided a noninvasive means for longitudinal evaluation of treatment efficacy (Fig. 6a). Thus, integrating NIR-II imaging

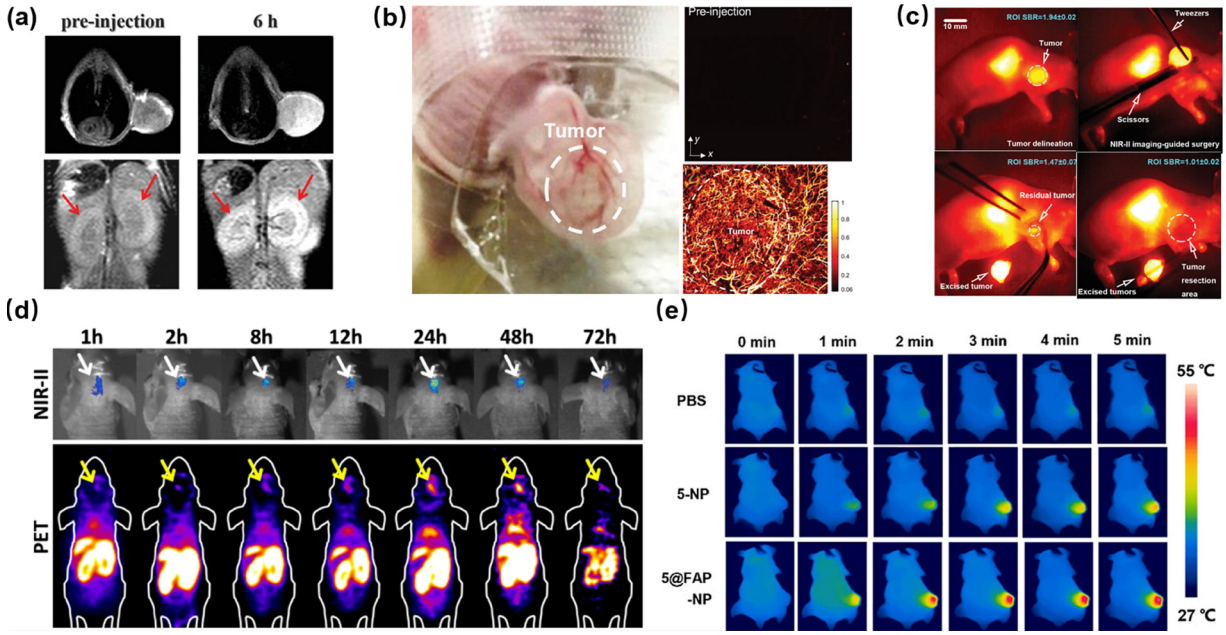

Fig. 6 (a) FMSN-MnO_2-BCQ enables *in vivo* dual-modal imaging and demonstrates antitumor efficacy in mice. Copyright 2021, John Wiley and Sons.[128] (b) PA imaging visualizes subcutaneous HepG2 tumors in mouse ears before and after PTD NP administration. Copyright 2019, John Wiley and Sons.[130] (c) NIR-II imaging with CH-4T/SLB–MSN–Mdot/Cu^{2+} guides A431 tumor detection and surgery 48 h post-injection. Copyright 2019, John Wiley and Sons.[26] (d) *In vivo* PET imaging post ^{64}Cu-DOTA-FA-ICG injection. Copyright 2022, John Springer Nature.[122] (e) IR thermal imaging of 4T1 tumors post-injection of PBS, 5-NP, or 5@FAP-NP with 880 nm laser irradiation. Copyright 2024, John Wiley and Sons.[39]

with MRI allows for more precise treatment guidance and helps minimize damage to non-malignant tissues.

5.2 NIR-II imaging combined with photoacoustic imaging

Photoacoustic imaging is a promising biomedical imaging modality that combines the excellent contrast of traditional optical imaging with the superb spatiotemporal resolution of ultrasound imaging.[129] It enables accurate localization of deep-seated tumors within the body, offering high-resolution and deep-penetration diagnostic capabilities. Zhang *et al.*[39] developed a multifunctional phototherapeutic small-molecule platform derived from an aza-BODIPY scaffold. Through the introduction of substituents with varied electron-donating and electron-withdrawing characteristics, followed by encapsulation within folic acid-functionalized polymeric carriers, the resulting nanostructure was capable of traversing the blood–brain barrier *via* receptor-mediated endocytosis and subsequently exhibiting selective affinity toward glioma cells (Fig. 6e). This system enabled NIR-II fluorescence/photoacoustic dual-modality imaging-guided PTT.

In the field of vascular imaging, NIR-II optical agents have also demonstrated excellent performance. Precise vascular imaging plays a vital role in the early diagnosis and therapeutic monitoring of diseases. Liu *et al.*[130] engineered conjugated polymer-based nanoparticles exhibiting intense NIR-II absorption, favorable biocompatibility, and robust photoacoustic stability. Their findings demonstrated that NIR-II-absorbing conjugated polymers can effectively support photoacoustic microscopy, enabling precise tumor margin definition as well as visualization of vascular networks within tumors and surrounding normal tissues (Fig. 6b). This work marked the first successful application of exogenous contrast agent-assisted NIR-II photoacoustic microscopy imaging.

5.3 NIR-II imaging combined with nuclear imaging

PET provides a functional complement to conventional anatomical imaging by visualizing tissue metabolism and biological activity. Through the detection of radiolabeled tracers administered at trace doses, PET delivers molecular-level information that aids in early disease detection and characterization. Its ability to perform whole-body scans further allows comprehensive lesion assessment, making it especially valuable in cancer staging and treatment monitoring. In contrast, NIR-II fluorescence imaging offers high spatial resolution and enhanced tissue penetration. Integrating PET with NIR-II fluorescence merges metabolic, functional, and anatomical information into a single multimodal platform, thereby significantly improving diagnostic accuracy. This synergy proves particularly impactful in surgical oncology. Dual-modality PET/NIR-II probes enable precise preoperative tumor localization and real-time intraoperative visual guidance. Together, these capabilities support more complete tumor resection while helping to minimize the risk of recurrence. Dual-modality NIR-II/PET probes exemplify the convergence of functional and optical imaging. For instance, an agent was constructed by Cheng *et al.* using biomimetic melanin nanoparticles, mesoporous silica, and a lipid bilayer, which co-encapsulated the NIR-II fluorophore CH-4T and the PET isotope ^{64}Cu.[26] This design enabled precise tumor visualization and

subsequently guided accurate surgical resection (Fig. 6c). In a parallel approach, Shi *et al.* engineered a folate receptor-α-targeted PET/NIR-II nanoprobe for glioblastoma.[131] The system demonstrated strong tumor selectivity and provided effective real-time fluorescence guidance during surgery, underscoring its potential for improving outcomes in precise tumor removal (Fig. 6d).

The integration of NIR-II optical agents with PET nuclear imaging presents a powerful multimodal strategy for enhancing diagnostic precision and guiding tumor surgery. To ensure its clinical viability, however, thorough assessment of *in vivo* safety, biocompatibility, and controlled biodegradation is essential to mitigate potential toxicity and prevent long-term accumulation. Comprehensive clinical investigations are therefore required to confirm both the efficacy and biosafety of NIR-II/PET platforms and to facilitate their translation into routine clinical practice.

5.4 NIR-II imaging combined with photothermal imaging

PTT is an emerging modality in cancer treatment. NIR photothermal nanomaterials have gained widespread attention in recent years due to the favorable tissue penetration of NIR light. Compared to the NIR-I, NIR-II makes it more promising for photothermal conversion applications. Mao *et al.*[132] prepared a series of gold nanorods (GNRs) with comparable aspect ratios and closely matched localized surface plasmon resonance (LSPR) characteristics. After surface functionalization with PEG and the tumor-targeting ligand lactoferrin, the resulting construct (GSE-HP) was further coated with a silica layer to improve optical transmission. Following structural modification, the absorption maximum exhibited a red shift from 810 nm to 846 nm while maintaining strong absorbance at the original 806 nm. Under 10-minute NIR irradiation, the system achieved a temperature rise of approximately 30 °C and demonstrated a photothermal conversion efficiency of 38.4%, reflecting excellent photothermal stability. In addition, the modified GNRs demonstrated rapid cellular internalization and pronounced *in vitro* photothermal cytotoxicity toward HepG2 cells. Follow-up studies using a mouse xenograft model confirmed effective tumor ablation upon exposure to 980 nm NIR light, underscoring the potential of these GNRs as efficient photothermal agents for cancer therapy within the NIR-II regime.

6. Remaining challenges toward clinical translation

6.1 Biosafety and long-term biocompatibility

NIR-II optical imaging technology employs optical agents for deep-tissue imaging. However, these agents often include QDs, metallic nanoparticles, and fluorescent dyes, which have raised widespread concerns about their biocompatibility and long-term safety in biomedical applications. Studies have shown that if NIR-II imaging agents cannot be effectively degraded *in vivo* or tend to accumulate in vital organs such as the liver and kidneys, they may trigger toxic reactions. For instance, QDs are widely used in NIR-II imaging due to their strong fluorescence performance, but the leakage of toxic heavy metal elements (*e.g.*, lead, cadmium) from their surfaces can cause significant biological toxicity. Similarly, metallic nanoparticles may interact with proteins in the blood, affecting their biodistribution and clearance rate. Therefore, in optimizing existing probes or designing novel NIR-II fluorophores, the primary objective should be to minimize or eliminate toxic components. Probe safety can be further enhanced by controlling particle size (*e.g.*, maintaining a diameter below 5 nm) and applying appropriate surface modifications to facilitate efficient renal clearance, thereby reducing the risk of systemic accumulation.[40]

Comprehensive toxicity assessment is essential to ensuring the clinical safety of NIR-II optical agents. Current evaluation strategies are broadly categorized into *in vitro* and *in vivo* approaches. *In vitro* studies typically involve exposing various cell types—such as hepatocytes or fibroblasts—to NIR-II agents to assess their effects on cell proliferation, migration, apoptosis, and overall viability. Additional indicators, including oxidative stress and DNA damage, provide insight into the mechanisms of intracellular biocompatibility. *In vivo* studies employ small animal models to investigate biodistribution, metabolism, tissue accumulation, and potential toxicity in major organs. These investigations help clarify clearance pathways and establish a theoretical foundation for safe clinical translation.

To improve the biocompatibility of NIR-II optical agents, recent research has focused on several key engineering strategies. Surface modification and specific ligand conjugation are widely used to enhance *in vivo* stability and biocompatibility. A prominent example is PEGylation, which reduces immune recognition of nanoparticles by shielding their surface, thereby significantly extending their circulation half-life.[69] Another important direction involves the design of biodegradable imaging agents. This includes certain organic nanomaterials and engineered QDs that are capable of gradual, natural breakdown within the body, preventing long-term accumulation.[133] Furthermore, targeted design plays a critical role in enhancing both imaging performance and biosafety. By conjugating specific targeting ligands, NIR-II agents can selectively accumulate at disease sites. This active targeting improves imaging contrast and accuracy while simultaneously minimizing off-target effects and reducing potential damage to healthy tissues.

Although NIR-II imaging surpasses conventional NIR-I methods in tissue penetration, acquiring high-quality images from deep anatomical regions remains a significant technical hurdle. This challenge can be addressed through parallel advancements in both probe design and imaging instrumentation. The performance of the fluorescent probe directly dictates achievable imaging depth and signal strength. Key strategies for probe optimization include engineering dyes or QDs with broad absorption, narrow emission profiles, high QY, and superior photostability, all of which enhance signal contrast and penetration capability. Furthermore, surface modifications that enable active targeting concentrate the probe specifically within diseased tissues, thereby amplifying the local signal and significantly improving image fidelity for deep-seated structures.[134–136]

Enhancing resolution represents another pivotal objective in advancing NIR-II imaging. By integrating NIR-II fluorescence with super-resolution microscopy techniques—such as stimulated emission depletion (STED) or structured illumination microscopy (SIM)—the diffraction limit inherent to conventional optical microscopy can be overcome. This synergy enables detailed visualization of subcellular structures, effectively bridging macroscopic tissue imaging with molecular- and cellular-scale analysis.[39,137] Consequently, the application scope of NIR-II imaging is expanding to encompass both systemic anatomical observation and high-resolution biological investigation.

Future progress in imaging hardware—including high-sensitivity detectors, improved spatial resolution, and advanced noise-reduction technologies—is anticipated to substantially enhance overall image quality. The development of compact, portable NIR-II imaging systems will be especially valuable for applications requiring real-time feedback, such as intraoperative guidance and longitudinal small-animal studies. In parallel, artificial intelligence (AI) is poised to transform image processing workflows. By integrating AI-driven algorithms for tasks such as image reconstruction, noise suppression, and automated resolution enhancement, NIR-II imaging can achieve greater precision, clarity, and diagnostic utility.

6.2 Current state of NIR-II imaging hardware

In addition to the development of high-performance NIR-II optical agents, advances in imaging hardware are equally important for achieving clinically translatable NIR-II imaging. Current NIR-II imaging systems generally consist of excitation sources, optical filters, imaging optics, image-processing software, and infrared-sensitive detectors. The synergistic optimization of these components critically determines imaging sensitivity, penetration depth, spatial resolution, temporal resolution, and intraoperative visualization capability.

Recent progress in NIR-II imaging hardware has substantially expanded the biomedical applications of NIR-II fluorescence imaging, including wide-field imaging, high-resolution microscopy, vascular imaging, image-guided surgery, and real-time intraoperative navigation. Compared with conventional visible and NIR-I imaging systems, NIR-II instrumentation benefits from reduced photon scattering, lower tissue autofluorescence, and improved imaging depth, thereby enabling high-contrast visualization of deep biological tissues.

Among all hardware components, detector performance plays the most critical role in determining overall imaging quality. Currently, indium gallium arsenide (InGaAs)-based cameras remain the gold-standard detectors for NIR-II imaging owing to their high quantum efficiency and sensitivity within the 900–1700 nm spectral range. Compared with conventional silicon-based charge-coupled device (CCD) and complementary metal-oxide-semiconductor (CMOS) detectors, InGaAs systems exhibit superior SWIR responsiveness and significantly enhanced deep-tissue imaging capability. Advanced detector architectures, including electron-multiplying CCD (EMCCD), intensified CCD (ICCD), and SWIR-CMOS systems, have also been explored to improve signal amplification, noise suppression, and real-time imaging performance.[138]

Nevertheless, current NIR-II detectors still face several technical limitations. InGaAs cameras are associated with high manufacturing cost, limited accessibility, relatively low pixel density, and increased thermal noise compared with visible-light imaging systems. In addition, detector cooling requirements and limited portability restrict their widespread implementation in routine clinical environments. These limitations remain major barriers to large-scale clinical translation of NIR-II imaging technologies.

Regarding excitation sources, 808 nm, 980 nm, and 1064 nm lasers are currently the most commonly employed excitation wavelengths in NIR-II imaging systems. Among them, 1064 nm excitation has attracted increasing attention because of its lower tissue scattering, reduced autofluorescence, and deeper tissue penetration capability. Simultaneously, advances in optical filtering systems, high-speed image acquisition modules, and AI-assisted image reconstruction algorithms have significantly improved image contrast, SNR, and real-time surgical navigation performance.

Importantly, recent studies have demonstrated the growing translational potential of NIR-II imaging hardware in clinical oncology, particularly in fluorescence-guided surgery, vascular imaging, lymph node mapping, and intraoperative tumor margin delineation. Several integrated NIR-II imaging platforms have already entered early-stage clinical evaluation, highlighting the feasibility of combining NIR-II optical agents with real-time imaging instrumentation for precision medicine applications.

Hardware and reconstruction optimization strategies are increasingly enhancing biomedical imaging performance. A panoramic needle-based EIT approach integrating hybrid transmission topology with spatially adaptive sensitivity compensation has been developed to overcome conventional field-of-view limitations, enabling robust real-time monitoring of IRE ablation boundaries with improved peripheral sensitivity and noise tolerance.[139]

Despite these advances, substantial challenges remain for the clinical implementation of NIR-II imaging hardware. Current systems still suffer from insufficient standardization of imaging parameters, lack of universally accepted calibration protocols, limited compatibility between imaging devices and fluorophore systems, and inadequate portability for routine surgical use. Therefore, future progress in NIR-II imaging is expected to rely on the coordinated evolution of optical agents, detector technologies, imaging software, clinically adaptable instrumentation platforms, AI and machine learning (ML).

AI and ML are emerging as promising computational tools for next-generation NIR-II imaging systems. Deep learning—based image restoration methods, including convolutional neural network (CNN) denoising, super-resolution reconstruction, and low-light enhancement algorithms, have demonstrated the ability to improve fluorescence image quality by suppressing noise and recovering structural details from photon-limited datasets.[140] For example, ensemble deep learning-assisted composite structured illumination

microscopy (eDL-cSIM) enables single-shot super-resolution reconstruction with improved robustness under low-SNR conditions, reduced reconstruction artifacts, and enhanced suitability for live-cell imaging.[141] Recently, AI-assisted NIR-II fluorescence molecular tomography (FMT) has been explored using a deep system prior—based graph convolution network (DSPGN), which incorporates graph-structured spatial priors and attention mechanisms into image reconstruction. This strategy improved fluorescence source localization and morphological recovery in both simulated and *in vivo* studies, demonstrating the potential of deep learning to enhance NIR-II image reconstruction quality and reduce ill-posedness in FMT.[142]

Such computational strategies may be particularly valuable for addressing current limitations of NIR-II detectors, including relatively low detector sensitivity, thermal noise, and restricted signal acquisition efficiency in low-photon imaging conditions. Although AI cannot fundamentally overcome hardware constraints or replace advances in detector materials (*e.g.*, InGaAs sensor optimization), it may partially compensate for sensitivity limitations through computational denoising, signal reconstruction, and enhanced feature extraction, thereby improving effective image usability and diagnostic interpretability (Table 2).

6.3 Clinical translation

Despite the rapid development of NIR-II optical agents, translational application remains significantly constrained by limited manufacturing standardization and insufficient evaluation of batch-to-batch reproducibility.[150] Compared with conventional small-molecule pharmaceuticals, many NIR-II agents involve complex multicomponent formulations, nanostructured assemblies, or biomimetic engineering strategies, which may introduce substantial variability during synthesis and scale-up production.

Among currently reported NIR-II agent classes, organic fluorophores generally exhibit relatively mature synthetic routes and higher production reproducibility due to their defined molecular structures and established purification procedures. In contrast, RENPs, QDs, and polymeric nanoplatforms often require multistep synthesis, ligand exchange, or self-assembly processes, which may lead to fluctuations in particle size, surface chemistry, fluorescence intensity, and colloidal stability across different batches.[151]

Dynamic light scattering (DLS) analysis and polydispersity index (PDI) measurements are among the most commonly reported indicators for evaluating formulation consistency.[152] In many studies, PDI values below 0.2 are considered indicative of acceptable monodispersity and batch uniformity. However, substantial heterogeneity still exists in the characterization standards adopted across different reports.[153] Several studies provide only single-batch physicochemical data without statistical validation of inter-batch reproducibility, which may limit translational reliability.[154]

Synthesis yield and scalability also vary considerably among different NIR-II agent systems. Small-molecule fluorophores and liposome-assisted formulations generally demonstrate relatively scalable preparation procedures, whereas biomimetic vesicles, cell membrane-coated nanoparticles, and multifunctional hybrid nanoplatforms often suffer from low production yield, complicated purification steps, and limited large-scale reproducibility.[155]

Importantly, only a limited number of NIR-II agents have been evaluated under GMP-compatible or GMP-like manufacturing conditions. Several clinically relevant formulations derived from FDA-approved materials, such as PEGylated dyes, liposomal systems, and ICG-based formulations, exhibit comparatively favorable translational potential due to their scalable synthesis strategies and established pharmaceutical manufacturing frameworks.[156] Nevertheless, standardized quality-

Table 2 Representative hardware components and characteristics of current NIR-II imaging systems

Hardware category	Representative system/device	Major advantages	Current limitations	Translational significance	Ref.
Infrared detector	InGaAs camera	High quantum efficiency; excellent SWIR sensitivity; deep tissue imaging capability	High cost; thermal noise; limited accessibility; relatively low pixel density	Currently the gold-standard detector for preclinical and early clinical NIR-II imaging	143
Infrared detector	SWIR-CMOS sensor	Faster acquisition speed; improved portability; lower power consumption	Lower sensitivity than InGaAs systems	Potential for portable and clinically adaptable imaging devices	144
Signal amplification detector	EMCCD/ICCD systems	Enhanced sensitivity and noise suppression	Complex integration; limited SWIR responsiveness	Useful for ultraweak fluorescence imaging applications	145
Excitation source	808 nm laser	Mature technology; broad fluorophore compatibility	Relatively shallow penetration depth	Widely used in conventional NIR-II imaging systems	146
Excitation source	980 nm laser	Improved tissue penetration	Water absorption-associated heating effects	Commonly used in nanoparticle excitation systems	147
Excitation source	1064 nm laser	Reduced scattering; lower autofluorescence; deeper penetration	Higher hardware requirements and cost	Increasingly important for clinically translatable NIR-II imaging	148
Imaging modality	Wide-field NIR-II imaging system	Large field-of-view; rapid imaging speed	Limited microscopic resolution	Suitable for intraoperative imaging and vascular visualization	149

Table 3 Manufacturing reproducibility and characterization considerations of representative NIR-II agent classes

Agent class	Typical synthesis yield	Batch variability	DLS/PDI consistency	Scalability	GMP-like production status	Ref.
Organic fluorophores	Moderate–high	Relatively low	Commonly reported; PDI usually <0.2	Good	Partial	157
RENPs	Moderate	Moderate	Size variation occasionally reported	Moderate	Rare	158
QDs	Low–moderate	Relatively high	Inconsistent reporting among studies	Limited	Rare	159
Polymeric nanoparticles	Variable	Assembly-dependent	DLS widely used for QC	Moderate	Limited	160
Biomimetic nanoplatforms	Low	High	Often insufficiently standardized	Poor	No established reports	161

control protocols, industrial-scale synthesis procedures, and regulatory manufacturing guidelines for most NIR-II agents remain insufficiently developed.

Future progress in NIR-II translational nanomedicine will require not only optimization of optical performance and targeting capability, but also rigorous batch-to-batch quality control, standardized physicochemical characterization, scalable manufacturing processes, and GMP-compatible production systems (Table 3).

7. Conclusions and future perspectives

NIR-II optical imaging has emerged as a highly promising technology for biomedical imaging and precision medicine owing to its reduced tissue scattering, low autofluorescence, deep penetration capability, and high spatiotemporal resolution. Recent advances in organic fluorophores, inorganic nanomaterials, rare-earth systems, and multimodal platforms have substantially expanded its applications in oncology, cardiovascular imaging, neuroscience, and image-guided intervention. However, accumulating evidence suggests that favorable optical properties alone are insufficient for clinical translation.

A major theme highlighted throughout this review is the transition from optical probes to translational optical agents. While probes provide intrinsic signal-generation capability, successful biomedical deployment requires additional optimization of physiological stability, pharmacokinetics, biosafety, targeting efficiency, and manufacturability. In this context, formulation engineering—including targeting modification, hydrophilicity regulation, size optimization, and carrier-assisted integration—has become a critical strategy for bridging material innovation with clinical applicability.

Despite substantial progress, several challenges remain. First, biosafety and long-term biocompatibility continue to limit the translation of many NIR-II systems, particularly inorganic and non-biodegradable nanomaterials. Second, current NIR-II imaging remains constrained by hardware limitations, including the high cost and limited accessibility of SWIR detectors and the lack of standardized imaging protocols. In addition, increasing platform complexity in multimodal and theranostic systems raises practical concerns regarding reproducibility, large-scale manufacturing, and regulatory evaluation.

Future development of NIR-II optical agents will likely focus on biodegradable and activatable systems with improved clearance behavior, stronger target specificity, and simplified translational design. Parallel advances in imaging hardware, portable devices, and artificial intelligence-assisted image analysis are expected to enhance quantitative imaging capability and clinical accessibility. Ultimately, continued integration of chemistry, materials science, engineering, and clinical medicine will be essential for accelerating the transition of NIR-II imaging from experimental research toward standardized precision diagnostics, image-guided surgery, and personalized healthcare.

Conflicts of interest

The authors declare that they have no known competing financial interests or personal relationships that could have appeared to influence the work reported in this paper.

Data availability

The data supporting the findings of this study are available within the article.

Acknowledgements

Q. Zou, L. Yang and W. Zhang contributed equally to this work. This work was supported by the National Key Research and Development Program of China (2023YFC2415700, 2023 YFB3810003), the National Natural Science Foundation of China (NSFC, No. 32571591, 825B2053), Xiang'an Innovation Laboratory Science and Technology Project (2024XAKJ0102008) and Xiamen Natural Science Foundation of China (3502Z2 02572009).

References

1 A. V. Naumova, M. Modo, A. Moore, C. E. Murry and J. A. Frank, *Nat. Biotechnol.*, 2014, **32**, 804–818.
2 G. Hong, A. L. Antaris and H. Dai, *Nat. Biomed. Eng.*, 2017, **1**, 0010.

3 S. Zhu, S. Herraiz, J. Yue, M. Zhang, H. Wan, Q. Yang, Z. Ma, Y. Wang, J. He and A. L. Antaris, *Adv. Mater.*, 2018, **30**, 1705799.
4 F. Wang, H. Wan, Z. Ma, Y. Zhong, Q. Sun, Y. Tian, L. Qu, H. Du, M. Zhang and L. Li, *Nat. Methods*, 2019, **16**, 545–552.
5 B. Guo, Z. Feng, D. Hu, S. Xu, E. Middha, Y. Pan, C. Liu, H. Zheng, J. Qian and Z. Sheng, *Adv. Mater.*, 2019, **31**, 1902504.
6 C. Li, Y. Zhang, M. Wang, Y. Zhang, G. Chen, L. Li, D. Wu and Q. Wang, *Biomaterials*, 2014, **35**, 393–400.
7 Z. Zhang, X. Fang, Z. Liu, H. Liu, D. Chen, S. He, J. Zheng, B. Yang, W. Qin and X. Zhang, *Angew. Chem., Int. Ed.*, 2020, **59**, 3691–3698.
8 Z. Cai, L. Zhu, M. Wang, A. W. Roe, W. Xi and J. Qian, *Theranostics*, 2020, **10**, 4265.
9 X. Hao, C. Li, Y. Zhang, H. Wang, G. Chen, M. Wang and Q. Wang, *Adv. Mater.*, 2018, **30**, 1804437.
10 A. M. Smith, M. C. Mancini and S. Nie, *Nat. Nanotechnol.*, 2009, **4**, 710–711.
11 Z. Feng, T. Tang, T. Wu, X. Yu, Y. Zhang, M. Wang, J. Zheng, Y. Ying, S. Chen and J. Zhou, *Light: Sci. Appl.*, 2021, **10**, 197.
12 M. Tanzid, N. J. Hogan, A. Sobhani, H. Robatjazi, A. K. Pediredla, A. Samaniego, A. Veeraraghavan and N. J. Halas, *ACS Photonics*, 2016, **3**, 1787–1793.
13 J. A. Carr, M. Aellen, D. Franke, P. T. So, O. T. Bruns and M. G. Bawendi, *Proc. Natl. Acad. Sci. U. S. A.*, 2018, **115**, 9080–9085.
14 S. Diao, J. L. Blackburn, G. Hong, A. L. Antaris, J. Chang, J. Z. Wu, B. Zhang, K. Cheng, C. J. Kuo and H. Dai, *Angew. Chem.*, 2015, **127**, 14971–14975.
15 O. T. Bruns, T. S. Bischof, D. K. Harris, D. Franke, Y. Shi, L. Riedemann, A. Bartelt, F. B. Jaworski, J. A. Carr and C. J. Rowlands, *Nat. Biomed. Eng.*, 2017, **1**, 0056.
16 L. Zheng, Y. Wu, Q. Wang, W. Du, L. Chen, J. Song and H. Yang, *Adv. Funct. Mater.*, 2024, **34**, 2407348.
17 S. Liu, S. Lu, S. Sun, J. Hai, G. Meng and B. Wang, *Anal. Chem.*, 2021, **93**, 14307–14316.
18 Z. Zhang, Y. Du, X. Shi, K. Wang, Q. Qu, Q. Liang, X. Ma, K. He, C. Chi and J. Tang, *Nat. Rev. Clin. Oncol.*, 2024, **21**, 449–467.
19 R. Tian, Q. Zeng, S. Zhu, J. Lau, S. Chandra, R. Ertsey, K. S. Hettie, T. Teraphongphom, Z. Hu and G. Niu, *Sci. Adv.*, 2019, **5**, eaaw0672.
20 Y. Jin, D. Li, X. Zheng, M. Gao, W. Wang, X. Zhang, W. Kang, C. Zhang, S. Wu and R. Dai, *Adv. Sci.*, 2024, **11**, 2308905.
21 H. Li, L. Zhu, Y. Zhang, L. Yang, W. Wu and D. Yang, *J. Controlled Release*, 2024, **366**, 28–43.
22 S. Zhang, B. Yang, H. Yang, J. Zhao, Y. Zhang, Y. Gao, O. Monteiro, K. Zhang, B. Liu and S. Wang, *Science Bulletin*, 2024, **69**, 1748–1756.
23 D. Zhou, G. Zhang, J. Li, Z. Zhuang, P. Shen, X. Fu, L. Wang, J. Qian, A. Qin and B. Z. Tang, *ACS Nano*, 2024, **18**, 25144–25154.
24 Y. Liu, H. Liu, H. Yan, Y. Liu, J. Zhang, W. Shan, P. Lai, H. Li, L. Ren and Z. Li, *Adv. Sci.*, 2019, **6**, 1801615.
25 L. Zhang, S. Xue, F. Ren, S. Huang, R. Zhou, Y. Wang, C. Zhou and Z. Li, *J. Nanobiotechnol.*, 2021, **19**, 296.
26 Q. Zhang, H. Zhou, H. Chen, X. Zhang, S. He, L. Ma, C. Qu, W. Fang, Y. Han and D. Wang, *Small*, 2019, **15**, 1903382.
27 I. J. Fox and E. H. Wood, *Mayo Clin. Proc.*, 1960, **35**, 732–744.
28 R. Weissleder, C.-H. Tung, U. Mahmood and A. Bogdanov, *Nat. Biotechnol.*, 1999, **17**, 375–378.
29 X. Gao, Y. Cui, R. M. Levenson, L. W. Chung and S. Nie, *Nat. Biotechnol.*, 2004, **22**, 969–976.
30 A. L. Antaris, H. Chen, K. Cheng, Y. Sun, G. Hong, C. Qu, S. Diao, Z. Deng, X. Hu and B. Zhang, *Nat. Mater.*, 2016, **15**, 235–242.
31 L. Cheng, C. Wang, L. Feng, K. Yang and Z. Liu, *Chem. Rev.*, 2014, **114**, 10869–10939.
32 N. K. Pandey, W. Xiong, L. Wang, W. Chen, B. Bui, J. Yang, E. Amador, M. Chen, C. Xing and A. A. Athavale, *Bioact. Mater.*, 2022, **7**, 112–125.
33 Z. Hu, C. Fang, B. Li, Z. Zhang, C. Cao, M. Cai, S. Su, X. Sun, X. Shi and C. Li, *Nat. Biomed. Eng.*, 2020, **4**, 259–271.
34 S. Wang, L. Liu, Y. Fan, A. M. El-Toni, M. S. Alhoshan, D. Li and F. Zhang, *Nano Lett.*, 2019, **19**, 2418–2427.
35 Y. Chang, H. Chen, X. Xie, Y. Wan, Q. Li, F. Wu, R. Yang, W. Wang and X. Kong, *Nat. Commun.*, 2023, **14**, 1079.
36 Y. Du, J. Xu, X. Zheng, Z. Dang, N. Zhu, Z. Jiang, J. Li and S. Zhu, *Adv. Mater.*, 2024, **36**, 2311515.
37 D. Liu, Z. He, W. Gao, J. Shang, Y. Yang, X. Zhang, X. Li, H. Ma and W. Shi, *Nat. Commun.*, 2025, **16**, 4911.
38 Y. Xiong, P. He, Y. Zhang, H. Chen, Y. Peng, P. He, J. Tian, H. Cheng, G. Liu and J. Li, *Regener. Biomater.*, 2023, **10**, rbac106.
39 Y. Song, X. Tong, Y. Han and Q. W. Zhang, *Aggregate*, 2025, **6**, e680.
40 C. Li, G. Chen, Y. Zhang, F. Wu and Q. Wang, *J. Am. Chem. Soc.*, 2020, **142**, 14789–14804.
41 J. Wang, Y. Xin, D. Chen, N. Zhang, Y. Xue, X. Liu, X. Li, W. Gao, Z. Hu and T. Sun, *Angew. Chem.*, 2025, **64**, e202507954.
42 O. Semenova, D. Kobzev, F. Yazbak, F. Nakonechny, O. Kolosova, A. Tatarets, G. Gellerman and L. Patsenker, *Dyes Pigm.*, 2021, **195**, 109745.
43 V. Dujols, F. Ford and A. W. Czarnik, *J. Am. Chem. Soc.*, 1997, **119**, 7386–7387.
44 L. Ding, X. Zhang, P. Wang, J. Ke, Y. Zhou, M. Wu, Z. Wei, Y. Cao, H. Li and G. Chen, *Nat. Commun.*, 2025, **16**, 8054.
45 X. Ge, Z.-M. Song, L. Sun, Y.-F. Yang, L. Shi, R. Si, W. Ren, X. Qiu and H. Wang, *Biomaterials*, 2016, **108**, 35–43.
46 Y. Yang, H. Zhang, Z. Yang and W. Huang, *Coord. Chem. Rev.*, 2026, **554**, 217598.
47 L. Wang, N. Li, W. Wang, A. Mei, J. Shao, W. Wang and X. Dong, *ACS Nano*, 2024, **18**, 4683–4703.
48 B. Li, J. Tian, C. Wu, Z. Li, L. Qiao, Z. Xie, B. Song, Y. Shan, S. Chen and Y. Tang, *Adv. Mater.*, 2024, **36**, 2405502.

49 G. Fang, D. Liu, M. Zhang, L. Shao, X. Shao, J. Chen, C. Meng, Y. Wang, K. Zeng and Q. Chen, *Coord. Chem. Rev.*, 2024, **504**, 215670.
50 J. Li, Z. Feng, X. Yu, D. Wu, T. Wu and J. Qian, *Coord. Chem. Rev.*, 2022, **472**, 214792.
51 Z. Hu, L. Feng and P. Yang, *Adv. Funct. Mater.*, 2024, **34**, 2310818.
52 E. D. Cosco, J. R. Caram, O. T. Bruns, D. Franke, R. A. Day, E. P. Farr, M. G. Bawendi and E. M. Sletten, *Angew. Chem., Int. Ed.*, 2017, **56**, 13126–13129.
53 J. Xu, N. Zhu, Y. Du, T. Han, X. Zheng, J. Li and S. Zhu, *Nat. Commun.*, 2024, **15**, 2845.
54 Z. Mao, H. Rha, J. Kim, X. You, F. Zhang, W. Tao and J. S. Kim, *Adv. Sci.*, 2023, **10**, 2301177.
55 H. N. Kim, M. H. Lee, H. J. Kim, J. S. Kim and J. Yoon, *Chem. Soc. Rev.*, 2008, **37**, 1465–1472.
56 W. E. Meador, E. Y. Lin, I. Lim, H. C. Friedman, D. Ndaleh, A. K. Shaik, N. I. Hammer, B. Yang, J. R. Caram and E. M. Sletten, *Nat. Chem.*, 2024, **16**, 970–978.
57 D. Gao, B. Zhang, Y. Liu, D. Hu, Z. Sheng, X. Zhang and Z. Yuan, *Theranostics*, 2019, **9**, 5315.
58 Z. Mao, J. H. Kim, J. Lee, H. Xiong, F. Zhang and J. S. Kim, *Coord. Chem. Rev.*, 2023, **476**, 214908.
59 S. Lee, S. Min, G. Kim and S. Lee, *Coord. Chem. Rev.*, 2024, **506**, 215719.
60 X. Hu, Z. Fang, C. Zhu, Y. Yang, Z. Yang and W. Huang, *Adv. Funct. Mater.*, 2024, **34**, 2401325.
61 X. Liu, B. Yu, Y. Shen and H. Cong, *Coord. Chem. Rev.*, 2022, **468**, 214609.
62 Y. Du, B. Xu, T. Fu, M. Cai, F. Li, Y. Zhang and Q. Wang, *J. Am. Chem. Soc.*, 2010, **132**, 1470–1471.
63 G. Hong, J. T. Robinson, Y. Zhang, S. Diao, A. L. Antaris, Q. Wang and H. Dai, *Angew. Chem., Int. Ed.*, 2012, **51**, 9818–9821.
64 Y. Zhang, Y. Liu, C. Li, X. Chen and Q. Wang, *J. Phys. Chem. C*, 2014, **118**, 4918–4923.
65 F. Sauvage, V. P. Nguyen, Y. Li, A. Harizaj, J. Sebag, D. Roels, V. Van Havere, K. Peynshaert, R. Xiong and J. C. Fraire, *Nat. Nanotechnol.*, 2022, **17**, 552–559.
66 K. Welsher, Z. Liu, S. P. Sherlock, J. T. Robinson, Z. Chen, D. Daranciang and H. Dai, *Nat. Nanotechnol.*, 2009, **4**, 773–780.
67 D. Ghosh, A. F. Bagley, Y. J. Na, M. J. Birrer, S. N. Bhatia and A. M. Belcher, *Proc. Natl. Acad. Sci. U. S. A.*, 2014, **111**, 13948–13953.
68 S. Bhattacharya, X. Gong, E. Wang, S. K. Dutta, J. R. Caplette, M. Son, F. T. Nguyen, M. S. Strano and D. Mukhopadhyay, *Cancer Res.*, 2019, **79**, 4515–4523.
69 M. L. Schipper, G. Iyer, A. L. Koh, Z. Cheng, Y. Ebenstein, A. Aharoni, S. Keren, L. A. Bentolila, J. Li and J. Rao, *Small*, 2009, **5**, 126–134.
70 X. Song, W. Zhu, X. Ge, R. Li, S. Li, X. Chen, J. Song, J. Xie, X. Chen and H. Yang, *Angew. Chem., Int. Ed.*, 2021, **60**, 1306–1312.
71 F. Wang and X. Liu, *J. Am. Chem. Soc.*, 2008, **130**, 5642–5643.
72 L. Cheng, K. Yang, Y. Li, J. Chen, C. Wang, M. Shao, S. T. Lee and Z. Liu, *Angew. Chem., Int. Ed.*, 2011, **50**, 7385–7390.
73 H. Zhao, H. Xiao, Y. Liu and H. Ju, *BMEMat*, 2023, **1**, e12032.
74 M. Kamimura, S. Takahiro, M. Yoshida, Y. Hashimoto, R. Fukushima and K. Soga, *Polym. J.*, 2017, **49**, 799–803.
75 M. Ye, X. Wang, J. Zou, W. Sun, W. Chi, Z. Mao and Z. Liu, *Nat. Commun.*, 2025, **16**, 8007.
76 H. Zhou, X. Zeng, A. Li, W. Zhou, L. Tang, W. Hu, Q. Fan, X. Meng, H. Deng and L. Duan, *Nat. Commun.*, 2020, **11**, 6183.
77 D. Wei, Y. Yu, Y. Huang, Y. Jiang, Y. Zhao, Z. Nie, F. Wang, W. Ma, Z. Yu and Y. Huang, *ACS Nano*, 2021, **15**, 5428–5438.
78 X. Zhang, S. Li, H. Ma, H. Wang, R. Zhang and X.-D. Zhang, *Theranostics*, 2022, **12**, 3345.
79 J. Zhu, C. Chu, D. Li, Y. Zhang, Y. Cheng, H. Lin, X. Wang, J. Liu, X. Pang and J. Cheng, *Front. Bioeng. Biotechnol.*, 2022, **10**, 890668.
80 H. Chen, H. Cheng, Q. Dai, Y. Cheng, Y. Zhang, D. Li, Y. Sun, J. Mao, K. Ren and C. Chu, *J. Controlled Release*, 2020, **323**, 635–643.
81 P. He, Y. Xiong, B. Luo, J. Liu, Y. Zhang, Y. Xiong, S. Su, C. Fang, Y. Peng and H. Cheng, *Bioeng. Transl. Med.*, 2023, **8**, e10404.
82 B. Li, M. Zhao, L. Feng, C. Dou, S. Ding, G. Zhou, L. Lu, H. Zhang, F. Chen and X. Li, *Nat. Commun.*, 2020, **11**, 3102.
83 W. Shi, S. Diao, T. Liang, X. Zhang, Z. Guo, Y. Liu, W. Zhou, C. Xie and Q. Fan, *ACS Appl. Bio Mater.*, 2022, **5**, 4965–4971.
84 J. Xu, T. Han, Y. Wang, F. Zhang, M. Li, L. Bai, X. Wang, B. Sun, X. Wang and J. Du, *Nano Lett.*, 2022, **22**, 7965–7975.
85 M. J. Whitley, D. M. Cardona, A. L. Lazarides, I. Spasojevic, J. M. Ferrer, J. Cahill, C.-L. Lee, M. Snuderl, D. G. Blazer III and E. S. Hwang, *Sci. Transl. Med.*, 2016, **8**, 320ra324.
86 J. Burggraaf, I. M. Kamerling, P. B. Gordon, L. Schrier, M. L. De Kam, A. J. Kales, R. Bendiksen, B. Indrevoll, R. M. Bjerke and S. A. Moestue, *Nat. Med.*, 2015, **21**, 955–961.
87 J. Li, F. Zhu, K. Lou, H. Tian, Q. Luo, Y. Dang, X. Liu, P. Wang and L. Wu, *Mater. Today Bio*, 2022, **16**, 100397.
88 C. Teng, H. Dang, Y. Xu, D. Yin and L. Yan, *Adv. Healthcare Mater.*, 2023, **12**, 2300541.
89 F. Liu, X. He, H. Chen, J. Zhang, H. Zhang and Z. Wang, *Nat. Commun.*, 2015, **6**, 8003.
90 L. Cheng, D. Jiang, A. Kamkaew, H. F. Valdovinos, H. J. Im, L. Feng, C. G. England, S. Goel, T. E. Barnhart and Z. Liu, *Adv. Funct. Mater.*, 2017, **27**, 1702928.
91 J. Zheng, B. Wu, F. Xu, T. Shan, X. Li, J. Tian and W. Zhang, *Biomaterials*, 2025, **317**, 123107.
92 S. Yang, N. Li, H. Xiao, G.-L. Wu, F. Liu, P. Qi, L. Tang, X. Tan and Q. Yang, *Theranostics*, 2022, **12**, 7853.
93 J. Zhang, K. Tang, Z. Liu, Z. Zhang, S. Duan, H. Wang, H. Yang, D. Yang and W. Fan, *Nanoscale Horiz.*, 2024, **9**, 186–214.

94 Z. Li, L. Du, B. Du, Z. Ullah, Y. Zhang, Y. Tu, Y. Zhou and B. Guo, *Theranostics*, 2025, **15**, 5616.
95 Y. Yu, D. Wei, T. Bing, Y. Wang, C. Liu and H. Xiao, *Adv. Mater.*, 2024, **36**, 2402452.
96 Y. Li, F. Qu, F. Wan, C. Zhong, J. Rao, Y. Liu, Z. Li, J. Zhu and Z. A. Li, *Nat. Commun.*, 2025, **16**, 762.
97 S. Gao, G. Wei, S. Zhang, B. Zheng, J. Xu, G. Chen, M. Li, S. Song, W. Fu and Z. Xiao, *Nat. Commun.*, 2019, **10**, 2206.
98 F. Wang, M. He, B. Huang, T. Tang, F. Liu, R. Cui, J. Qian, M. Zhang and T. Sun, *Anal. Chem.*, 2023, **95**, 10947–10956.
99 Global Burden of Cardiovascular Diseases and Risks 2023 Collaborators, *J. Am. Coll. Cardiol.*, 2025, **86**, 2167–2243.
100 G. Hong, J. C. Lee, J. T. Robinson, U. Raaz, L. Xie, N. F. Huang, J. P. Cooke and H. Dai, *Nat. Med.*, 2012, **18**, 1841–1846.
101 Y. Wu, C. Wang, J. Guo, A. Carvalho, Y. Yao, P. Sun and Q. Fan, *Biomater. Sci.*, 2020, **8**, 4438–4446.
102 G. Hong, J. C. Lee, A. Jha, S. Diao, K. H. Nakayama, L. Hou, T. C. Doyle, J. T. Robinson, A. L. Antaris and H. Dai, *Circ.:Cardiovasc. Imaging*, 2014, **7**, 517–525.
103 Z. Jiang, X. Geng, L. Su, A. Chen, Z. Sheng and T. Jiang, *Mater. Today Chem.*, 2022, **26**, 101062.
104 S. H. Lee, O.-K. Kim, S. Lee and J. K. Kim, *Spectrochim. Acta, Part A*, 2018, **205**, 132–138.
105 D. Goldstein, R. H. El-Maraghi, P. Hammel, V. Heinemann, V. Kunzmann, J. Sastre, W. Scheithauer, S. Siena, J. Tabernero and L. Teixeira, *J. Natl. Cancer Inst.*, 2015, **107**, dju413.
106 D. Papadatos-Pastos, K. Thillai, R. Rabbie, P. Ross and D. Sarker, *Expert Rev. Anticancer Ther.*, 2014, **14**, 1115–1125.
107 Q. Xie, J. Liu, B. Chen, X. Ge, X. Zhang, S. Gao, Q. Ma and J. Song, *ACS Appl. Bio Mater.*, 2022, **5**, 711–722.
108 H. Zhou, W. Yi, A. Li, B. Wang, Q. Ding, L. Xue, X. Zeng, Y. Feng, Q. Li and T. Wang, *Adv. Healthcare Mater.*, 2020, **9**, 1901224.
109 H. Lou, A. Ji, C. Qu, S. Duan, H. Liu, H. Chen and Z. Cheng, *Chem. Eng. J.*, 2022, **449**, 137848.
110 P. Wang, Y. Fan, L. Lu, L. Liu, L. Fan, M. Zhao, Y. Xie, C. Xu and F. Zhang, *Nat. Commun.*, 2018, **9**, 2898.
111 Y.-Y. Zhu, L. Song, Y.-Q. Zhang, W.-L. Liu, W.-L. Chen, W.-L. Gao, L.-X. Zhang, J.-Z. Wang, Z.-H. Ming and Y. Zhang, *Cancer Res.*, 2023, **83**, 3428–3441.
112 X. Zhou, Q. Liu, W. Yuan, Z. Li, Y. Xu, W. Feng, C. Xu and F. Li, *Adv. Sci.*, 2021, **8**, 2000441.
113 M. Grossi, M. Morgunova, S. Cheung, D. Scholz, E. Conroy, M. Terrile, A. Panarella, J. C. Simpson, W. M. Gallagher and D. F. O'Shea, *Nat. Commun.*, 2016, **7**, 10855.
114 H. Wan, J. Yue, S. Zhu, T. Uno, X. Zhang, Q. Yang, K. Yu, G. Hong, J. Wang and L. Li, *Nat. Commun.*, 2018, **9**, 1171.
115 R. R. Zhang, A. B. Schroeder, J. J. Grudzinski, E. L. Rosenthal, J. M. Warram, A. N. Pinchuk, K. W. Eliceiri, J. S. Kuo and J. P. Weichert, *Nat. Rev. Clin. Oncol.*, 2017, **14**, 347–364.
116 A. L. Vahrmeijer, M. Hutteman, J. R. Van Der Vorst, C. J. Van De Velde and J. V. Frangioni, Nature reviews, *Clin. Oncol.*, 2013, **10**, 507–518.
117 M. Zhang, Z. Wang, C. Wang, Y. Wu, Z. Li and Z. Liu, *ACS Nano*, 2021, **15**, 11940–11952.
118 J. Miao, M. Miao, Y. Jiang, M. Zhao, Q. Li, Y. Zhang, Y. An, K. Pu and Q. Miao, *Angew. Chem., Int. Ed.*, 2023, **62**, e202216351.
119 S. Wang, H. Shi, L. Wang, A. Loredo, S. M. Bachilo, W. Wu, Z. Tian, Y. Chen, R. B. Weisman and X. Zhang, *J. Am. Chem. Soc.*, 2022, **144**, 23668–23676.
120 M. Zhao, W. Lai, B. Li, T. Bai, C. Liu, Y. Lin, S. An, L. Guo, L. Li and J. Wang, *Angew. Chem., Int. Ed.*, 2024, **63**, e202403968.
121 J. Wang, P. Shangguan, X. Chen, Y. Zhong, M. Lin, M. He, Y. Liu, Y. Zhou, X. Pang and L. Han, *Nat. Commun.*, 2024, **15**, 705.
122 K. He, J. Zhou, F. Yang, C. Chi, H. Li, Y. Mao, B. Hui, K. Wang, J. Tian and J. Wang, *Theranostics*, 2018, **8**, 304.
123 K. He, P. Li, Z. Zhang, J. Liu, P. Liu, S. Gong, C. Chi, P. Liu, C. Chen and J. Tian, *Eur. J. Nucl. Med. Mol. Imaging*, 2022, **49**, 2929–2937.
124 Q. Qu, H. Nie, S. Hou, F. Wang, K. He, P. Deng, S. Chen, Z. Zhang, C. Chi and Z. Hu, *Eur. J. Nucl. Med. Mol. Imaging*, 2022, **49**, 4752–4754.
125 C. W. Barth, S. Z. H. Rizvi, A. M. Masillati, S. Chakraborty, L. G. Wang, A. R. Montaño, D. A. Szafran, W. S. Greer, N. S. van den Berg and J. Sorger, *Small*, 2024, **20**, 2300011.
126 Z. Feng, Y. Yang, J. Zhang, K. Wang, Y. Li, H. Xu, Z. Wang, E. Biskup, S. Dong and X. Yang, *Nano Res.*, 2019, **12**, 3059–3068.
127 S. Y. Lee, S. I. Jeon, S. Jung, I. J. Chung and C.-H. Ahn, *Adv. Drug Delivery Rev.*, 2014, **76**, 60–78.
128 Z. Zheng, Z. Jia, C. Qu, R. Dai, Y. Qin, S. Rong, Y. Liu, Z. Cheng and R. Zhang, *Small*, 2021, **17**, 2006508.
129 K. Wilson, K. Homan and S. Emelianov, *Nat. Commun.*, 2012, **3**, 618.
130 B. Guo, J. Chen, N. Chen, E. Middha, S. Xu, Y. Pan, M. Wu, K. Li, C. Liu and B. Liu, *Adv. Mater.*, 2019, **31**, 1808355.
131 X. Shi, P. Xu, C. Cao, Z. Cheng, J. Tian and Z. Hu, *Eur. J. Nucl. Med. Mol. Imaging*, 2022, **49**, 4325–4337.
132 H. Yang, H. He, Z. Tong, H. Xia, Z. Mao and C. Gao, *J. Colloid Interface Sci.*, 2020, **565**, 186–196.
133 T. Pan, D. Lu, H. Xin and B. Li, *Light: Sci. Appl.*, 2021, **10**, 124.
134 Z. Feng, Y. Li, S. Chen, J. Li, T. Wu, Y. Ying, J. Zheng, Y. Zhang, J. Zhang and X. Fan, *Nat. Commun.*, 2023, **14**, 5017.
135 A. Ji, H. Lou, C. Qu, W. Lu, Y. Hao, J. Li, Y. Wu, T. Chang, H. Chen and Z. Cheng, *Nat. Commun.*, 2022, **13**, 3815.
136 N. D. Calvert, J. Baxter, A. A. Torrens, J. Thompson, A. Kirby, J. Walia, S. Ntais, E. Hemmer, P. Berini and B. Hibbert, *Nat. Nanotechnol.*, 2025, **20**, 276–285.
137 F. Wang, Y. Zhong, O. Bruns, Y. Liang and H. Dai, *Nat. Photonics*, 2024, **18**, 535–547.
138 B. Zhu and H. Jonathan, *Sensors*, 2024, **24**, 3539.
139 L. Zhao, Y. Shu, S. Xiang, C. Yao and S. Dong, *Appl. Phys. Lett.*, 2026, 128.
140 M. Weigert, U. Schmidt, T. Boothe, A. Müller, A. Dibrov, A. Jain, B. Wilhelm, D. Schmidt, C. Broaddus and S. Culley, *Nat. Methods*, 2018, **15**, 1090–1097.
141 J. Qian, C. Wang, H. Wu, Q. Chen and C. Zuo, *PhotoniX*, 2025, **6**, 13.

142 B. Wang, S. Li, H. Zhang, J. Li, L. Zhang, J. Yu, X. He and H. Guo, *Comput. Methods Programs Biomed.*, 2025, 108948.
143 S. Zhu, R. Tian, A. L. Antaris, X. Chen and H. Dai, *Adv. Mater.*, 2019, **31**, 1900321.
144 R. H. Wilson, G. T. Kennedy, C. A. Campbell, T. Phan, A. H. Lin, B. Levi and A. J. Durkin, *J. Biomed. Opt.*, 2026, **31**, 010901.
145 E. Ciarrocchi and N. Belcari, *EJNMMI Phys.*, 2017, **4**, 14.
146 J. A. Carr, D. Franke, J. R. Caram, C. F. Perkinson, M. Saif, V. Askoxylakis, M. Datta, D. Fukumura, R. K. Jain and M. G. Bawendi, *Proc. Natl. Acad. Sci. U. S. A.*, 2018, **115**, 4465–4470.
147 Y.-F. Wang, G.-Y. Liu, L.-D. Sun, J.-W. Xiao, J.-C. Zhou and C.-H. Yan, *ACS Nano*, 2013, **7**, 7200–7206.
148 L. A. Sordillo, Y. Pu, S. Pratavieira, Y. Budansky and R. R. Alfano, *J. Biomed. Opt.*, 2014, **19**, 056004.
149 B. Zhu and E. Sevick-Muraca, *Br. J. Radiol.*, 2015, **88**, 20140547.
150 P. J. Gawne, M. Ferreira, M. Papaluca, J. Grimm and P. Decuzzi, *Nat. Rev. Mater.*, 2023, **8**, 783–798.
151 K. R. Sims, J. P. Maceren, A. I. Strand, B. He, C. Overby and D. S. Benoit, *RSC Adv.*, 2020, **10**, 2513–2518.
152 M. R. Zamani Kouhpanji and B. J. Stadler, *Sensors*, 2020, **20**, 2554.
153 S. M. Stavis, J. A. Fagan, M. Stopa and J. A. Liddle, *ACS Appl. Nano Mater.*, 2018, **1**, 4358–4385.
154 C. Saunders, C. A. de Villiers and M. M. Stevens, *AAPS J.*, 2023, **25**, 94.
155 R. Paliwal, R. J. Babu and S. Palakurthi, *AAPS PharmSciTech*, 2014, **15**, 1527–1534.
156 S. B. Patel and D. P. Sanap, *OpenNano*, 2026, 100288.
157 M. Danaei, M. Dehghankhold, S. Ataei, F. Hasanzadeh Davarani, R. Javanmard, A. Dokhani, S. Khorasani and Y. M. Mozafari, *Pharmaceutics*, 2018, **10**, 57.
158 G. Wang, Q. Peng and Y. Li, *Acc. Chem. Res.*, 2011, **44**, 322–332.
159 J. S. Lee, Y. H. Youn, I. K. Kwon and N. R. Ko, *J. Pharm. Invest.*, 2018, **48**, 209–214.
160 S. Mitragotri, T. Lammers, Y. H. Bae, S. Schwendeman, S. C. De Smedt, J. C. Leroux, D. Peer, I. C. Kwon, H. Harashima and A. Kikuchi, *J. Controlled Release*, 2017, **246**, 183–184.
161 R. H. Fang, A. V. Kroll, W. Gao and L. Zhang, *Adv. Mater.*, 2018, **30**, 1706759.